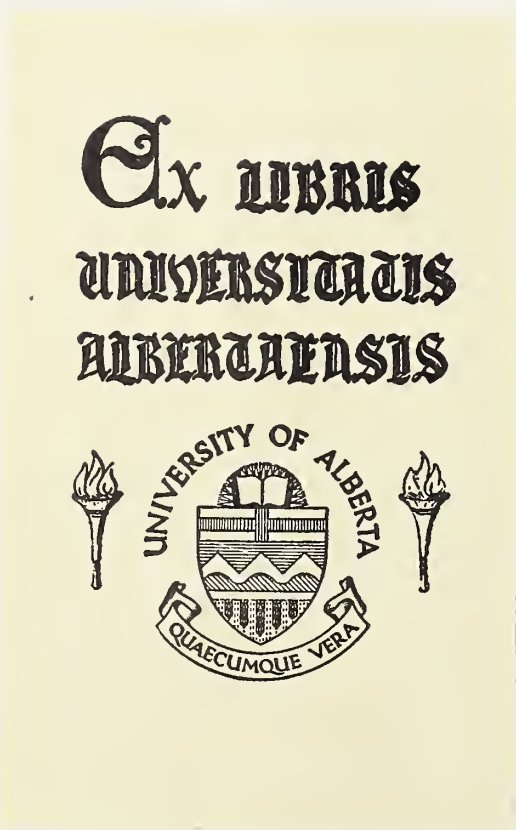

THE UNIVERSITY OF ALBERTA

# PRETENSIONED BEAMS WITH CONFINED COMPRESSED CONCRETE

by

ROBERT LYLE WARD

A THESIS

SUBMITTED TO THE FACULTY OF GRADUATE STUDIES

IN PARTIAL FULFILMENT OF THE REQUIREMENTS FOR THE DEGREE OF

MASTER OF SCIENCE

DEPARTMENT OF CIVIL ENGINEERING

EDMONTON, ALBERTA

APRIL, 1966

## ABSTRACT

The object of this investigation was to study the influence of concrete confinement on the behavior of bonded, prestressed beams subjected to bending. The effects of type and amount of confinement, amount of tension reinforcement and concrete strength on the load-deflection and moment-curvature relationships were studied.

Twelve beams having a 6 x 14-5/8 in. cross-section and a 10-in. effective depth were tested. All of the beams were loaded at two points symmetrically about midspan.

From the test data, load-deflection and moment-curvature relationships were derived. Theoretical moment-curvature relationships prior to spalling were derived and compared to the observed relationships. Observed moment-curvature relationships were also compared to the moment-curvature relationships for similar beams with unconfined concrete.

The tests indicated that the presence of confining reinforcement, even prior to spalling, influenced the load-deformation relationships. Confinement of the concrete was found to be a very effective means of improving the moment-rotation characteristics of prestressed beams which under normal conditions were over-reinforced.

ACKNOWLEDGEMENTS

This investigation was made possible through funds and facilities provided by the Department of Civil Engineering together with financial assistance given by the National Research Council of Canada.

This investigation was supervised by Dr. J. Warwaruk, Associate Professor in the Department of Civil Engineering. His assistance in planning the test series and preparing the manuscript is sincerely appreciated.

The author also wishes to thank:

Messrs. H. Panse and B. Aves for their assistance in fabrication and testing of the beams.

Messrs. D. McGowan and C.G. Blunck for fabrication of equipment.

Mr. J.R.V. Walters for his assistance in testing of the specimens.

Miss H. Wozniuk for typing the manuscript.

TABLE OF CONTENTS

LIST OF TABLES

LIST OF FIGURES

LIST OF FIGURES (Continued)

# CHAPTER I

# INTRODUCTION

## 1.1 Introductory Remarks

The work reported in this thesis is an exploratory investigation into the deformation characteristics of pretensioned prestressed concrete beams with bound concrete in the compression zone. Although several investigations on the deformation characteristics of normal reinforced and prestressed beams (5),(6),(8)* are presented in the literature, only few reports (1),(2),(3) are available of tests conducted on bound concrete beams.

The limit design of any structure is based on a sound knowledge of the rotational capacity of the members which make up the structure. Concrete members which are over-reinforced and are of rectangular prestressed section tend to fail in a brittle manner. It is, therefore, necessary to improve the moment-rotational characteristics of such members before they can be designed for a structure using limit design procedures. The increase in ductility required can be obtained by lateral confinement of the compressed concrete.

A limited number of investigations have been carried out on the behavior of bound concrete under axial and eccentric load, and on the behavior of beams with bound concrete. Several of these investigations

---

*Numbers in parenthesis refer to entries in the List of References.

are discussed in the next chapter.

## 1.2 Object

The primary object of this investigation was to study the effects of lateral confinement of the compressed concrete on the load-deformation characteristics of beams failing mainly in flexure. The first phase of the investigation was carried out to study the influence of two types of spiral confinement with spiral pitch remaining constant. The second phase was a study of the influence of variations of spiral pitch.

The major variables in this study were:

(a) type of confinement

(b) amount of confinement

(c) concrete strength

(d) amount of tension reinforcement

Although the level of prestress was meant to be a constant slight unintentional variation did occur throughout the three series of beams tested.

Strains over the depth of the beam and beam deflections were measured. From this data, moment-curvature and load-midspan deflection relationships were obtained and the effects of the variables on these relationships were studied.

Theoretical moment-curvature relationships at loads prior to spalling, assuming no spiral influence, were derived and compared to those obtained from measurement of strains over the depth of the beam.

## 1.3 Scope

The investigation included tests of three series of beams. The

first series consisted of Beams A1 to A4, the second, Beams B1 to B4 and the third, Beams C1 to C4. All of the beams had a rectangular cross-section measuring 6 x 14-5/8-in. and an effective depth of 10-in. Beams A1 and B1 had an 11-ft. span length and all other beams had a 10-ft. span. All of the beams were loaded at two points symmetrical about centerline. The length of the constant moment region was 5-ft. for beams A1 and B1 and 4-ft. for all other beams. Beams of Series A and Series B were reinforced with 6 and 8 seven-wire strands of 5/16-in. nominal diameter; all of the beams of Series C had 8 strands. The lateral confinement in all beams was derived from spirals formed from No. 2 plain reinforcing bars.

Beams A1 to A4 had a single 6-in. O.D. spiral in the compressive zone. Concrete strengths of approximately 5000 and 3200 psi were used. For each concrete strength percentages of tension reinforcement of 0.578 and 0.770 were used.

Beams B1 to B4 were similar in all respects to Beams A1 to A4 except that confinement was obtained by the use of two smaller spirals in the top of the beams. Beam B1 had two 3-in. O.D. spirals and Beams B2 to B4 had two 4-in. O.D., overlapping spirals. By combining the first two series it was possible to obtain one large series to study the effects of the type of spiral used.

Beams of Series C were of two concrete strengths. For each concrete strength of approximately 4900 and 3600 psi, a 2 and 3-in. pitch was used for the single 6-in. O.D. spiral in the compression zone.

The deformation characteristics, as determined from tests of twelve beams, are reported in this thesis. Comparisons are made between

the results of these tests and the tests of similar beams without confinement carried out by previous investigators at the University of Alberta (5),(6). Although an analysis of the bound beam section is beyond the scope of this thesis, suggestions are presented as a guide to future investigators.

# CHAPTER II

# REVIEW OF RESEARCH

## 2.1 Introduction

Research to date on the behavior of concrete beams has been concentrated mainly on testing and analysis of beams having no bound concrete in the compression zone. Extensive work has been done on the strength and deformation characteristics of reinforced concrete beams and various similar investigations have been conducted on prestressed concrete beams. The investigations most pertinent to this paper are discussed in following discussions.

Information is also available in the literature on various investigations carried out on bound concrete columns. The use of spiral reinforcement in columns results in more ductile failures and a reserve strength after spalling under proper design.

More recent investigations have been carried out on eccentrically loaded bound concrete members and attempts made to predict the "hinging" properties of helically bound concrete sections. Only a limited number of reports are available of tests conducted on beams having bound compression zones.

## 2.2 Research on Prestressed Beams Without Bound Concrete

Tests at the University of Illinois (8) were carried out on 82 beams. A study of various variables and conditions of bond was carried

out to facilitate methods of predicting beam behavior. Procedures for determining flexural deformations through the use of moment-curvature relationships were developed. Recent investigations at the University of Alberta by Raffa (6) and Belke (5) were carried out to study flexural strength, load-deflection and moment-curvature relationships for rectangular, one and two-point loaded, prestressed beams. The result of extensive research to date has made it possible to predict with reasonable accuracy the load capacity and load-deformation relationships which might be expected from any ordinary prestressed beam during service conditions or during loading to failure.

## 2.3 Research an Axially-Loaded Confined Concrete

Tests by F.E. Richart, A. Brandtzaeg and R.L. Brown, reported by Blume (4) were carried out on laterally confined, axially-loaded concrete cylinders. Test results indicated that the following expression related the axial load and applied lateral pressure:

$$\nabla_a = f'_c + 4.1\nabla_\ell$$

where $\nabla_a$ = axial strength

$f'_c$ = strength of unconfined specimen

$\nabla_\ell$ = lateral confining pressure

The lateral confining pressure term was modified in terms of spiral dimension and stress. It was found also that by replacing $f'_c$ with $0.85f'_c$ the expression so derived was representative of tests carried out. The resulting expression for an axially-loaded, spirally reinforced

column is:

$$f_c = 0.85f'_c + \frac{8.2A''_s f''_s}{a\ \overline{D}} \ *$$

Although this expression is not directly applicable for eccentrically loaded columns, it is an indication of the strength of a concrete member that can be expected through the use of confinement.

## 2.4 Research on the Behavior of Bound Concrete

Various investigators have presented, through analytical and experimental means, stress-strain relationships for bound concrete. The essential difference, between the stress-strain relationships for bound and unbound concrete, is the increase of stress resistance that can be derived from the bound concrete at very high plastic strains.

A general stress-strain curve for bound concrete, as given by Chan in Reference (3), is shown in FIGURE 2.1. The elastic stage of the concrete may be assumed to be represented by the portion of the curve between O and A and the plastic stage by portion ABC of the curve. The ultimate strain $\epsilon_u$ , is small for unbound concrete and $\lambda_2$ is usually negative. The behavior of bound concrete is much the same as that for unbound concrete through portion OAB. Beyond this stage lateral deformations of bound concrete induce tension stresses in the confining spiral reinforcement and with adequate confinement $\lambda_2$ can be positive. This positive slope of the bound concrete stress-strain curve beyond point B, which represents spalling in a beam, causes a delay in failure and allows

*Notations are defined in APPENDIX A.

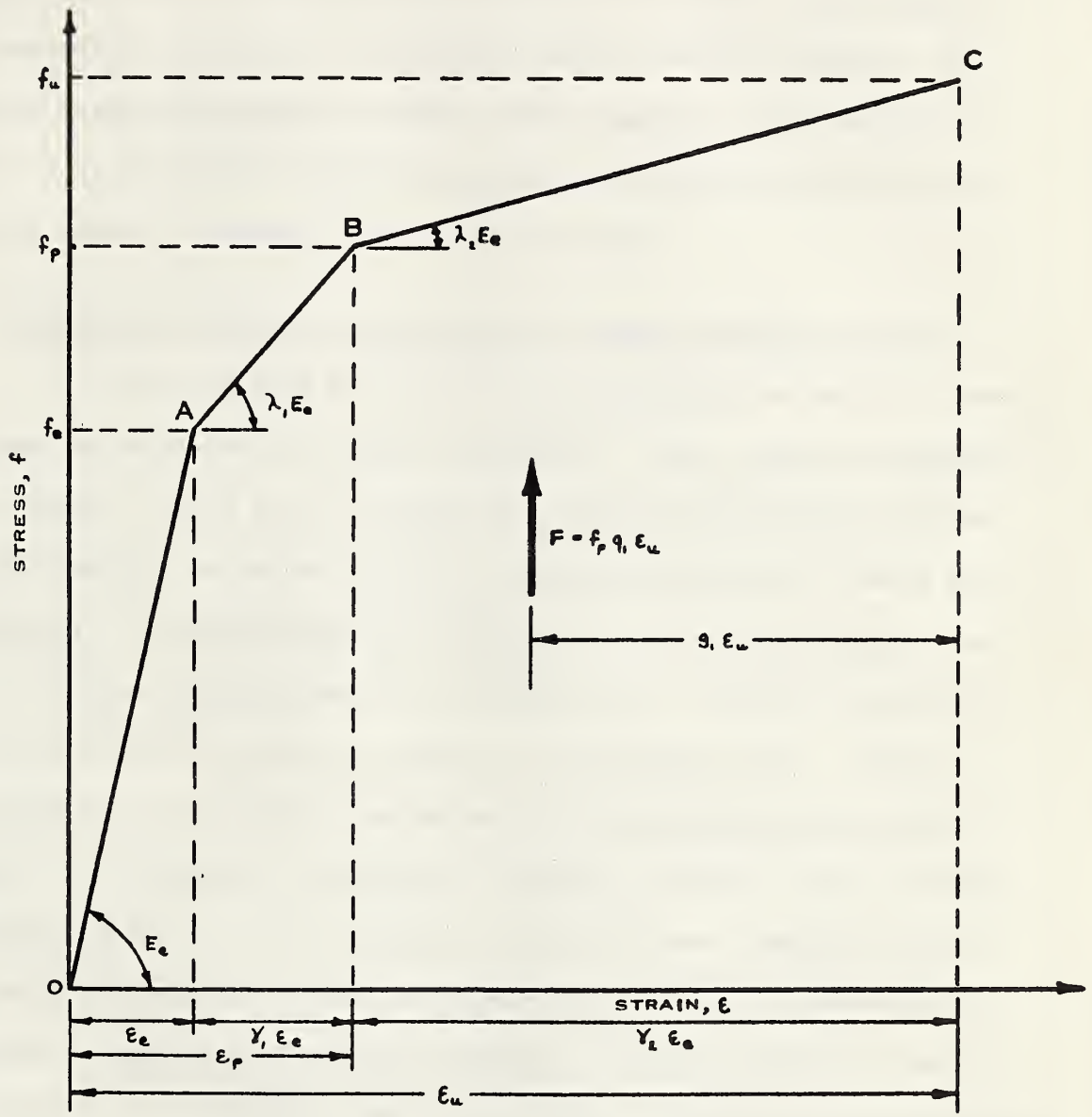


FIGURE 2.1 GENERAL STRESS-STRAIN RELATIONSHIP FOR BOUND CONCRETE(3)

high plastic deformations to occur. An ultimate strain much higher than the strain at failure for unbound concrete can also be obtained. Chan suggests that if the constants associated with FIGURE 2.1 are known it is possible to determine the resultant force F and its location. By substituting the appropriate values of the resultant force and its location into the usual equations of equilibrium and compatibility it is then possible to analyse a bound concrete beam.

## 2.5 Research on Behavior of Bound Concrete Under Combined Loading

Tests conducted by Chan (3) were carried out on axially-loaded confined circular and rectangular specimens. Three series of specimens were tested. Series B and C consisted of short bound specimens pinned at both ends and subjected to axial compression loading at a small eccentricity. This simulated the conditions of the confined compression zone of a beam failing primarily in compression. The main variables in these two series were type and amount of confinement used. Series S consisted of test specimens loaded axially through pinned ends with a transverse load applied at midspan. Each half of these loaded specimens therefore represented the compression zone core under combined bending and axial loadings which would be present in a beam with tension reinforcement, single-point loaded at midspan. The main variable in Series S was the ratio of bending load to axial load. By varying the axial load it was possible to study the influence of axial load on the length of the plastic zone and the nature of curvature distribution. The axial load was kept sufficiently high to ensure primary compression failure in all specimen tests.

Among the observations made during these tests were the following:

(a) Ultimate strain of unbound concrete varied from .003 to .004 in./in. under the action of combined bending and axial loads.

(b) The reduction in concrete compression area associated with spalling caused an abrupt drop in load capacity, but the lateral confinement enabled the concrete core to continue to resist load.

(c) Lateral binding prevented brittle collapse that is associated with compression failures in ordinary beams.

(d) Where there was a strain gradient along the member, spalling propagated from the point of maximum strain to points of lesser strain as loading continued.

(e) Prior to spalling the binding had little or no effect on beam behavior.

(f) Compression failures occurred either by failure of the concrete arching between the adjacent binding loops or by excessive dilation of the binding reinforcement.

(g) Circular binding was much more efficient than rectangular binding in supplying lateral support.

Curves were also plotted to express the relation between the ultimate equivalent concrete stress at failure and the lateral binding ratio and between ultimate concrete strain and the lateral binding ratio. The lateral binding ratio is defined as the volume of binder divided by the volume of bound concrete. These plots indicate that with adequate

binding the ultimate equivalent concrete stress could be as high as 1.8 times the compressive strength if circular binding is used and 1.3 times the compressive strength for rectangular binding. Ultimate strains could be as high as 0.025 in./in. for circular binding and 0.018 for rectangular binding.

The following equations were presented to represent these curves:

Ultimate equivalent concrete stress factor, $K_u = \frac{q_u f_p}{c_u}$

$P_b = 0.0375 (K_u - K_o)^2$ (circular binding)

$P_b = 0.189 (K_u - K_o)^2$ (rectangular binding)

where $K_o = 0.696$ (circular binding)

$K_o = 0.82$ (rectangular binding)

Ultimate strain, $\epsilon_u$

$P_b = 4{,}970 (\epsilon_u - \epsilon_o)^3$ (circular binding)

$P_b = 14{,}600 (\epsilon_u - \epsilon_o)^3$ (rectangular binding)

where $\epsilon_o = 0.0035$ (for both circular and rectangular binding).

A discussion of the effects of confinement of a beam cross-section due to stirrup reinforcing is presented in Reference (4). The magnitude of confinement obtained from rectangular binding of this form has been shown to be small compared to that which is possible through introduction of circular binding in the compression zone of the beam (3)(1).

The effects of variations in stirrup reinforcement shall, therefore, be neglected for purposes of comparisons in this paper.

## 2.6 Research on Moment-Rotation of Beams With Confined Concrete

Tests of 16, single-point loaded beams, 13 of which were ordinarily reinforced and 3 prestressed, are reported by Base and Read (1) of Great Britain. The series of tests was conducted to study the efficiency of helical reinforcement in the compression zone as a means of improving the moment-rotation characteristics of the plastic hinges that formed in the confined core.

Main steel in the reinforced concrete beams was varied so that failures would normally have been those of under-reinforced, balanced and over-reinforced beams. Various combinations of stirrup reinforcement and helical reinforcements were used to compare the effectiveness of each in confining the compression zone concrete. Circular confinement was supplied by two 3-1/4-in. outside diameter overlapping helices. At later stages of loading a constant deflection apparatus was used to apply deflection increments. The reduction in load resistance of the beams at the constant sustained deflections were observed. In this manner load-deflection and moment-rotation curves were obtained up to and beyond the peak load. It was felt that this type of loading simulated the conditions occurring in a plastic hinge in a structure as the hinge is being forced to rotate owing to deformation of adjacent parts of the structure under increasing load.

The results of these tests indicated that helical reinforcement

was generally more efficient and economical than stirrups in rectangular beams. This was due to the tendency of the rectangular stirrups to deform outward and therefore permit compression zone crushing. The various forms of confinement had little or no influence on the behavior of the beams in the elastic range and did not prevent or delay significantly the formation of crushing cracks on the compression surface.

For the prestressed beams tested the load at initial compression failure was found to be considerably larger than the estimated ultimate load. This discrepancy was believed to be due to the increased moment of resistance at the loaded section as a consequence of the triaxial state of compression that existed under the loading plates, and to the fact that the compression zone movement, down from the top of the beam at the loaded section towards the bottom of the beam at the supports, appeared to result in an additional confining effect.

Conclusions presented on the basis of these tests were that:

(a) Under-reinforced beams probably have enough plasticity at failure and should not need lateral confinement in the region of plastic hinges.

(b) Balanced section reinforced concrete beams fail in a brittle manner unless the compression zone in the region of the plastic hinge is bound. Helical binding transforms the brittle bending failure into the ideal plastic failure with the hinge moment or resistance nearly constant for a large rotation.

(c) A combination of helices and closely spaced stirrups is required to produce ideal characteristics of failure and

rotation in over-reinforced beams. Helical reinforcement delays the shear collapse to some extent in the absence of sufficient stirrup reinforcement.

(d) In beams with a high percentage of reinforcement in the tension region the effect of helical binding is to increase the maximum moment of resistance of the plastic hinge to a value significantly higher than a similar beam without binding.

(e) Rectangular prestressed beams are particularly lacking in plasticity at failure. Helical binding is an economical and effective way of producing satisfactory plastic failure characteristics.

Base (2) tested two similar two-point loaded ordinarily reinforced beams prior to the time of the above investigation (1). Both beams were tension reinforced with mild steel, one beam having unbound compression zone concrete and the other having 2 - 2-3/4-in.O.D. helices in the compression zone.

The two beams behaved in almost identical manners up to spalling. Crushing then occurred in the ordinary beam and as deformation was applied the depth of crushing zone increased and moment of resistance decreased rapidly. Concrete spalled from the outside of the helix in the second beam, accompanied by a slight decrease in the resisting moment. The beam then carried increasing load at high deflections after the spalling was complete. The results of this investigation showed that it was possible, by the inclusion of helical reinforcement to contain the com-

pression zone of a concrete beam, and obtain a very large rotational capacity without a large reduction in moment resistance.

The majority of the beam tests reported in References (1), (2) and (3) were conducted on ordinary reinforced beams. Since the behavior of an ordinary reinforced beam is very similar to the behavior of a prestressed beam at loads approaching ultimate and in regions beyond initial spalling, the results of these tests will, for the most part, apply to prestressed beams with bound compression zone concrete.

# CHAPTER III

# MATERIALS, FABRICATION AND TEST PROCEDURES

## 3.1 Materials

### 3.1.1 Cement

All beams were cast using Type III, high-early strength, Portland Cement. The cement was purchased in one lot from a local Manufacturer and stored under proper conditions in the laboratory.

### 3.1.2 Aggregates

Aggregates were obtained from a local supplier. The coarse aggregate was 3/8-in. pea-gravel and was delivered to the laboratory in a dry condition. The sand was delivered in a saturated condition with a moisture content at delivery of 5%. Gradual drying reduced this moisture content during laboratory storage. The results of sieve analyses of the aggregates are shown in TABLE 3.1. Fineness Modulus of the sand was found to be 2.55.

### 3.1.3 Concrete Mixes

Concrete mix design was carried out according to the method outlined by the Portland Cement Association, (10). Trial batches were prepared prior to casting of the test beams and air-cured under laboratory conditions. Adjustments to design mixes were then made on the basis of 3-day compressive strengths.

Concrete properties and strengths for each test specimen are

TABLE 3.1

SIEVE ANALYSIS OF AGGREGATES

| FINE AGGREGATE | | | COARSE AGGREGATE | | |
|---|---|---|---|---|---|
| Sieve | % Retained | Cumulative % Retained | Sieve | % Retained | Cumulative % Retained |
| #4 | 8.2 | 8.2 | 3/4 | 0 | 0 |
| #8 | 11.1 | 19.3 | 3/8 | 5.9 | 5.9 |
| #16 | 6.5 | 25.8 | #4 | 87.1 | 93.0 |
| #30 | 7.3 | 33.1 | Pan | 7.0 | 100.0 |
| #50 | 42.3 | 75.4 | | | |
| #100 | 17.3 | 92.7 | | | |
| Pan | 1.8 | -- | | | |
| Silt | 5.5 | -- | | | |
| Total | 100.0 | 254.5 | | 100.0 | 198.9 |

given in TABLE 3.2. Due to progressive drying of the aggregates and non-uniformity of moisture content throughout the aggregate in storage, the mixing water was adjusted from beam to beam on the basis of visual inspection and slump tests. Compressive strengths were obtained from tests of standard 6 x 12-in. control cylinders at each of 3 and 7 days after casting of the beams. On the day of a beam test two standard cylinders were tested in compression and two were tested in splitting to obtain tensile strengths. The modulus of rupture was determined from tests of 4-1/2 x 3-1/2 x 16-in. control beams loaded at the third-points of a 12-in. span.

3.1.4 Reinforcement

3.1.4(a) Prestressing Strand - The prestressing strand used for tension reinforcement was a seven-wire, high-strength, nominal 5/16-in. diameter strand. This strand is designated as "Seven-Wire Uncoated Stress-Relieved" and meets ASTM A-416 specifications. All strand was from one lot. The stress-strain relationship for this strand as determined by the manufacturer is shown in FIGURE 3.1.

3.1.4(b) Shear Reinforcement - Shear reinforcement used in the beams was either No. 2 plain or No. 3 deformed bent bars.

3.1.4(c) Spiral Reinforcement - The various spirals that were placed in the test beams were fabricated from No. 2 plain bars. The bars used for this purpose were purchased in one lot from a local supplier. The load-strain relationship for a sample of this reinforcement was determined for the as-supplied condition and moderately cold-worked condition resulting from spiral forming operation. The two relationships

TABLE 3.2

CONCRETE STRENGTHS AND PROPERTIES

| Beam No. | Cement:Sand: Gravel by weight | Water/ Cement by weight | Slump (in.) | Compressive Strength (psi) | | Tensile Strength (psi) | | Modulus of Rupture (psi) | | Age At test (days) | Compressive Strength 3 day | 7 days |
|---|---|---|---|---|---|---|---|---|---|---|---|---|
| | | | | 1 | 2 | 1 | 2 | 1 | 2 | | (psi) | |
| A1 | 1:3.1:2.2 | 0.72 | 5 1/2 | 4670 | 5020 | 370 | - | 560 | 610 | 13 | 2980 | 4370 |
| A2 | 1:3.1:2.2 | 0.78 | 5 | 5170 | 4920 | 450 | 320 | 815 | 678 | 32 | 3530 | 4130 |
| A3 | 1:4.4:2.9 | 0.95 | 3 1/2 | 3220 | 3220 | 294 | - | 569 | 584 | 34 | 1730 | 2300 |
| A4 | 1:4.4:2.9 | 0.91 | 4 | 3320 | 3440 | 337 | 352 | 589 | 621 | 29 | 1660 | 8 day 2930 |
| B1 | 1:3.1:2.2 | 0.69 | 4 | 5170 | 5030 | 347 | 378 | 621 | 632 | 27 | 3470 | 4220 |
| B2 | 1:3.1:2.2 | 0.75 | 4 | 4820 | 4710 | 398 | 399 | 713 | 763 | 35 | 3210 | 4070 |
| B3 | 1:4.4:2.9 | 1.03 | 4 1/2 | 2970 | 3110 | 300 | 351 | 589 | 567 | 32 | 1710 | 2340 |
| B4 | 1:4.4:2.9 | 0.88 | 5 | 3100 | 3160 | 308 | 327 | 610 | 617 | 31 | 2000 | 8 day 2690 |
| C1 | 1:3.1:2.2 | 0.75 | 3 1/2 | 4850 | 4930 | 414 | 403 | 728 | 698 | 26 | 3410 | 4250 |
| C2 | 1:3.1:2.2 | 0.75 | 3 3/4 | 4820 | 4940 | 415 | 406 | 682 | 632 | 27 | 3370 | -- |
| C3 | 1:4.4:2.9 | 0.92 | 4 | 3540 | 3570 | 325 | 316 | 665 | 698 | 36 | 2180 | 8 day 2970 |
| C4 | 1:4.4:2.9 | 0.93 | 3 1/2 | 3560 | 3620 | 399 | 342 | 665 | 687 | 35 | 2150 | 8 day 2970 |

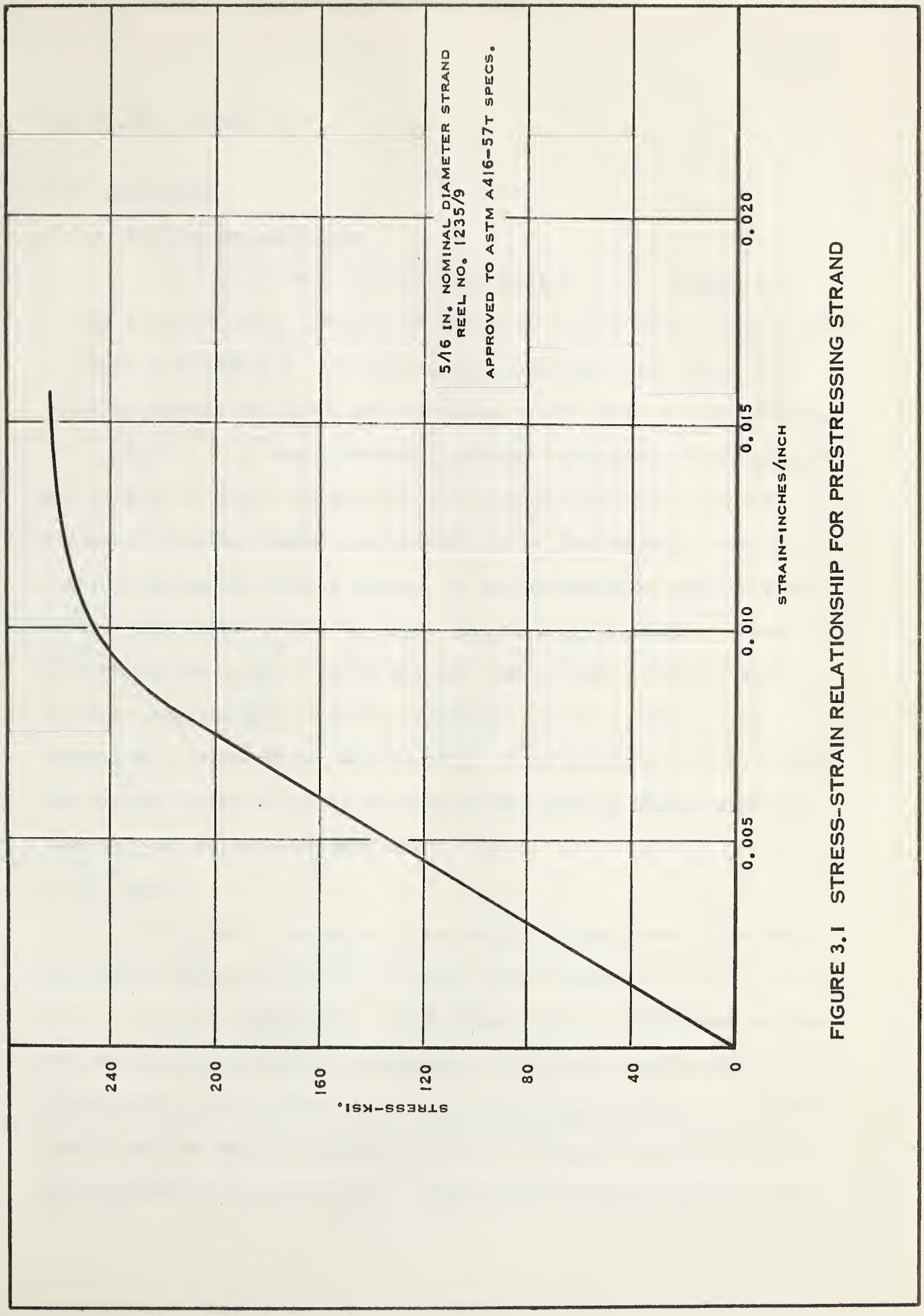


FIGURE 3.1 STRESS-STRAIN RELATIONSHIP FOR PRESTRESSING STRAND

are shown in FIGURE 3.2.

## 3.2 Fabrication

### 3.2.1 Fabrication of Spirals

The spirals were fabricated by winding the No. 2 plain bars around a rotating pipe fixed in the chucks of a steel lathe. This process is shown in FIGURE 3.3. All spirals were wound initially with a 1-in. pitch by setting the travel per revolution of the lathe to 1-in. Spirals of 2 and 3-in. pitch were subsequently formed by hand from those obtained by using the lathe to acquire the desired pitch and outside diameter. Because of elastic rebound that occurred after the release of tension in the rods during the winding process, it was necessary to experiment with various pipe sizes to find the right size to give the desired outside diameter on the spiral. The pipe sizes used to wind the 3-in., 4-in., and 6-in. spirals were 2-1/4-in., 3-1/2-in. and 5-in. respectively. Twenty-foot lengths of bar were wound at a time giving one spiral section. The desired length of spiral was made by butt welding several sections together with an oxy-acetylene torch.

### 3.2.2 Forms

Beams were cast in pairs in two 12'-6" long forms. The forms were fabricated using two 12-in. channel sides bolted at two foot intervals to an 18-in. channel base. End plates were also of channel sections and were drilled with holes to accomodate the strand reinforcement. Large C-clamps were used to secure these end plates in position. To obtain a depth of section greater than 12-in. the forms were modified by the introduction of two 3 x 4-in. nominal size wood members between the

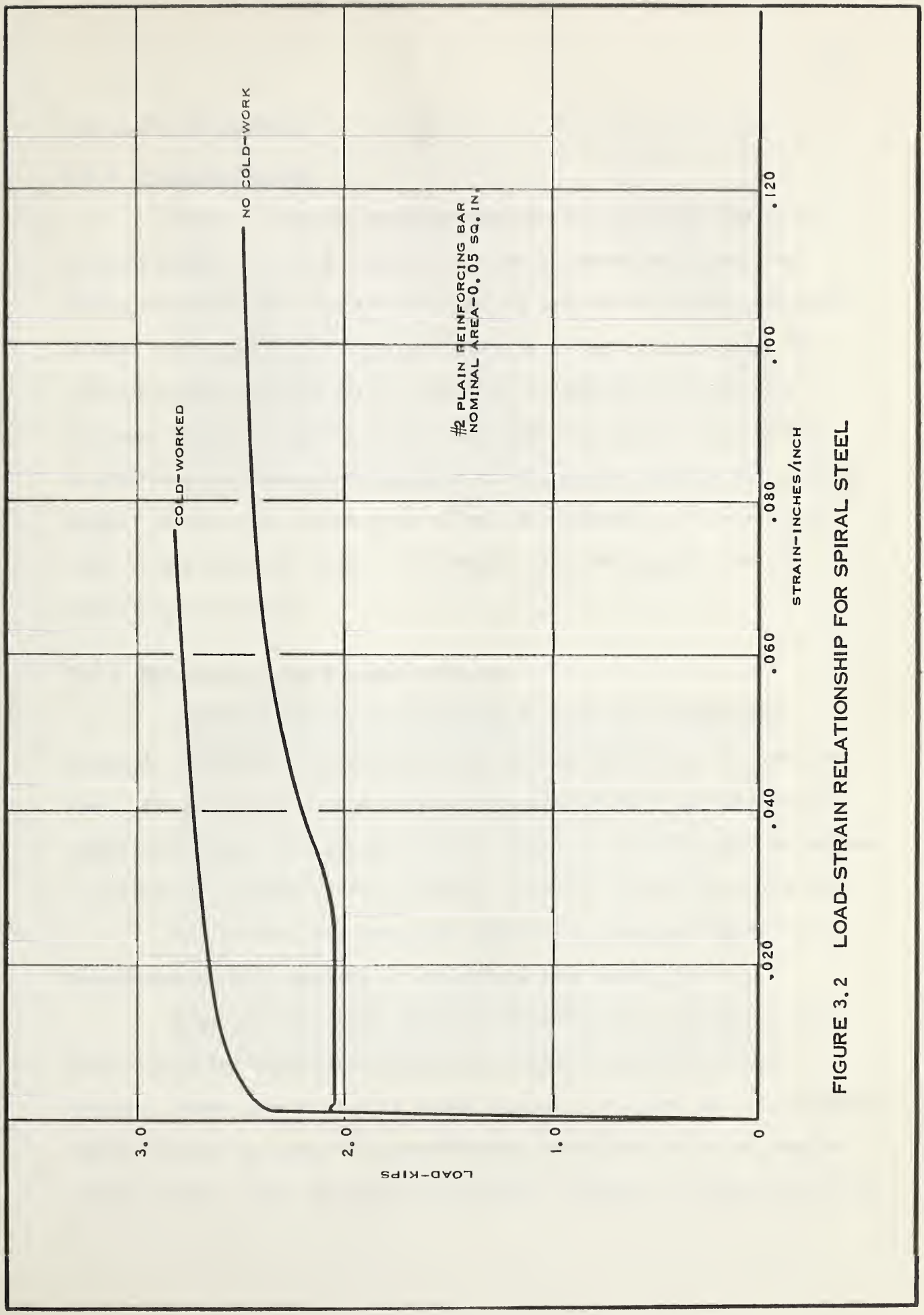


FIGURE 3.2 LOAD-STRAIN RELATIONSHIP FOR SPIRAL STEEL

side and base channels.

3.2.3 Prestressing Bed

Reactions for the prestressing operation were supplied by two existing movable concrete bulkheads. These bulkheads were placed in mortor and anchored to the loading floor by four prestressed anchor bolts. A clear distance of 28-ft. between bulkheads allowed the placement of two beam forms in series with a reasonable working space between the bulkheads and the forms and between the forms themselves. The ability to prestress two beams simultaneously in this manner resulted in increased control of the level of prestress as well as uniformity of the initial level of prestress for each pair of beams. The casting time was also significantly reduced.

3.2.4 Prestressing and Forming Operation

With only the two channel bases in place the strands were threaded through the form end plates and through end plates at each bulkhead. The end plates at the bulkhead were drilled with the appropriate number and spacing of holes and, when centered at the bulkheads, maintained the proper configuration of the strands during the prestressing operation.

The strands were tensioned individually using a Simplex center-hole hydraulic jack operated by a Blackhawk hand pump.

Wedge-grip end anchorages were used to grip the strand. These grips consist of three wedge shaped jaws inside a tapered cylindrical housing. These jaws are spring loaded against a threaded end cap. Wedging action between the jaws and tapered housing, upon application of tension to the strand, causes gripping to take place. FIGURE 3.4 shows the jacking

FIGURE 3.3 FORMING SPIRAL SECTIONS
ON THE LATHE

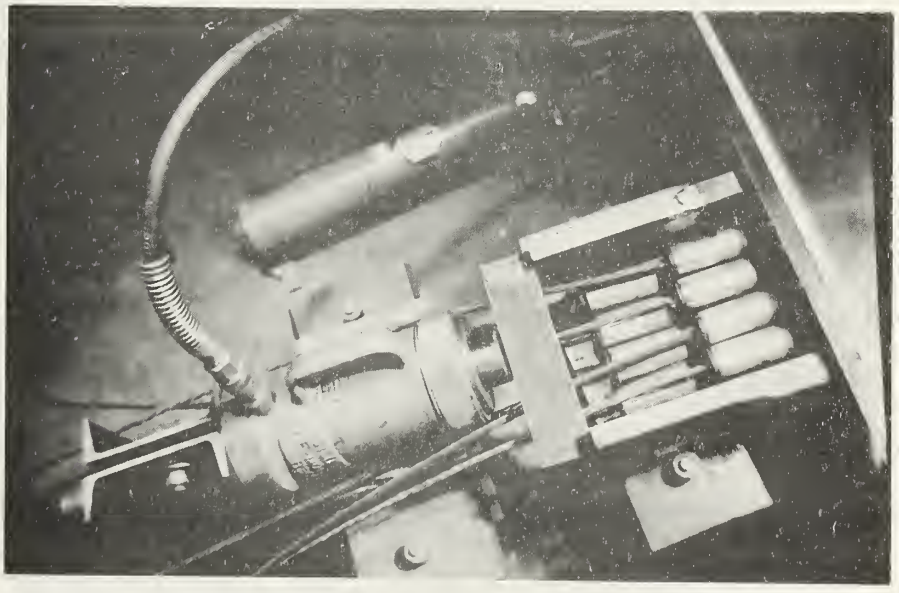

FIGURE 3.4 JACKING ARRANGEMENT
AND GRIPS
[NORTH BULKHEAD]

arrangement and grips in place at the north bulkhead.

Special aluminum dynamometers, shown in FIGURE 3.5, were used to measure the tension in each strand. These dynamometers were inserted between the grip end and the end plate at the south bulkhead. Strains in the dynamometers were measured using two A7 SR-4 electrical strain gages wired in series. Each dynamometer was load tested and existing calibration charts checked prior to the start of prestressing. These calibration charts were then used to relate the strains to the force in the strand. The strains required to obtain the desired level of initial prestress were calculated prior to prestressing and pre-set on the strain indicator. Grips were set on the jacking end of the strands when this level of prestress was reached and minor adjustments were made to account for slip in the grips by the use of thin shims. FIGURE 3.6 shows the prestressing bed just after completion of strand tensioning.

After all the strands had been stressed the shear reinforcement was fixed in place by wiring the stirrups directly to the tension strands. The base of each form was then levelled at the proper elevation. The side forms were erected and bolted in place and the end sections positioned and clamped in place. The stirrups were next fastened in an upright position by wiring them to a No. 3 reinforcing bar supported above the forms. These wires were cut and the top bar removed after the concrete had been placed. FIGURE 3.7 shows the assembled form with stirrups and top bar in place.

Spiral reinforcement was not placed in the beams until the concrete in the lower portion of the forms had been placed and vibrated.

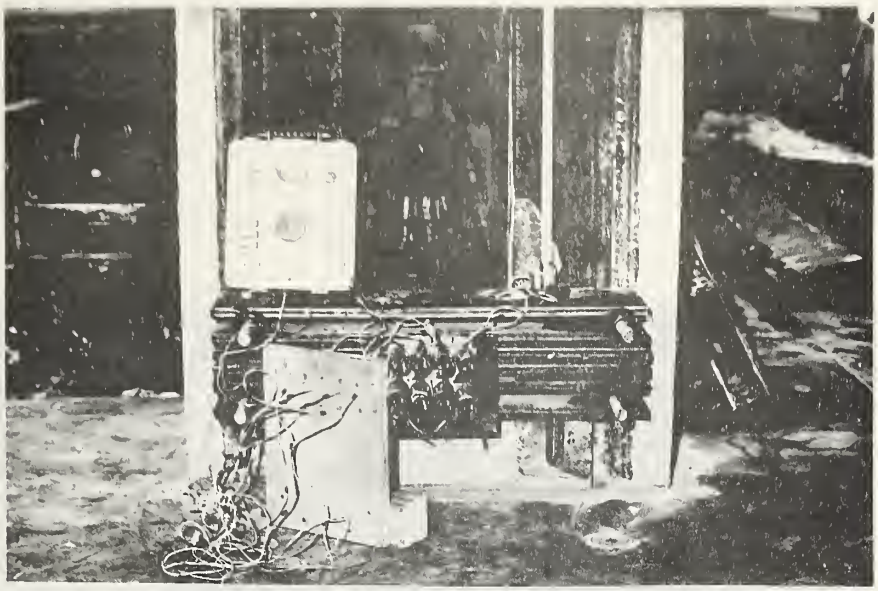

FIGURE 3.5 STRAIN INDICATOR AND DYNAMOMETERS

[SOUTH BULKHEAD]

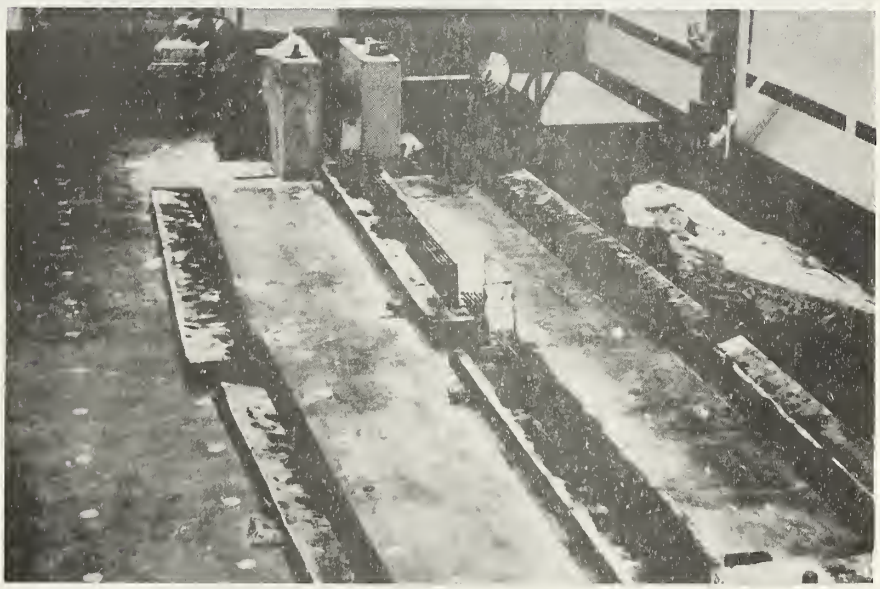

FIGURE 3.6 TENSIONED STRANDS PRIOR TO ASSEMBLY OF FORMS

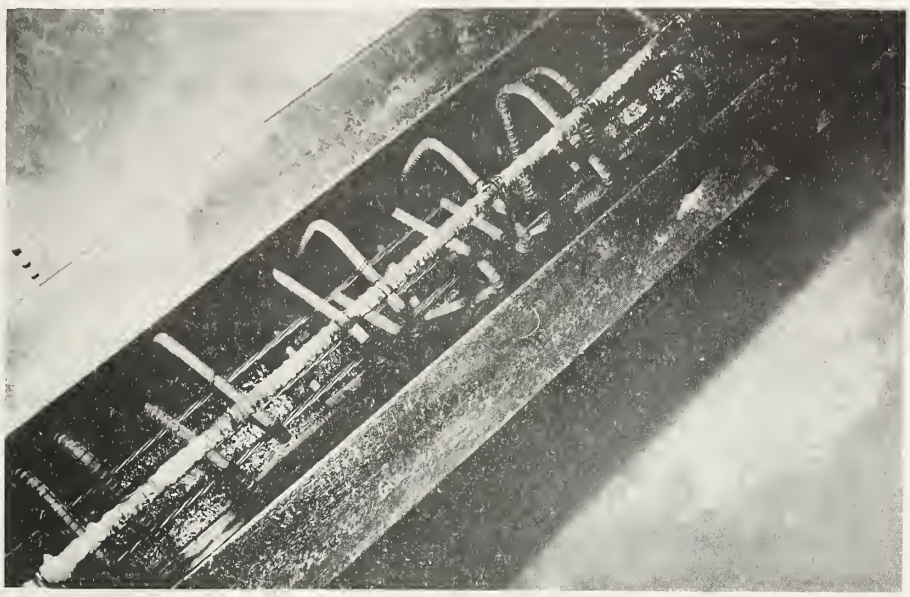

FIGURE 3.7 ASSEMBLED FORM WITH STIRRUPS AND TOP BAR IN PLACE

The spiral was then placed in the form with the welds at the bottom and the remainder of the concrete placed and vibrated. The welds were placed at the bottom of the spiral to ensure that they would be located at position of least stress.

3.2.5 Casting and Curing

Concrete was mixed in a 9 cu. ft. capacity upright mixer. Three batches of approximately 6-1/2 cu. ft. were used to cast the two beams. The first batch was placed in the end regions of the two beams and the second and third batches were placed in the center sections of each beam. This was done to insure uniformity of the concrete in the constant moment region between the load points.

A butter mix of approximately 1-1/2 cu. ft. was made prior to mixing of the three large batches. Slump tests were made on each batch before placing of the concrete in the beams. The concrete was placed and compacted with an immersion type high frequency vibrator.

Two 4-1/2 x 3-1/2 x 16-in. control beams and six 6 x 12-in. control cylinders were cast from the concrete batch used in the middle section of each beam. These control specimens were tested in the manner outlined previously in Section 3.1.3.

After the concrete had set, the beams and control specimens were covered with saturated burlap and a polythene sheet. The forms were removed after 24 hours and the concrete again covered. Moist curing was continued for three days after which time the beams were removed from the prestressing bed. They were then air cured in the laboratory until the time of test.

The release of prestress was carried out four days after casting. A cutting torch was used to heat the strands in the region between the two beams. The reduction in stress in the cables, as a result of creep at elevated temperatures, effected a gradual transfer of stress from the strands to the concrete.

Prior to the release of prestress, gage points were attached to each beam along the longitudinal centerline on the top surface and at the level of the tension reinforcement on the side surface. Initial readings were then measured along these gage lines with an 8-in. Demec deformation gage. Readings were again taken after the completion of prestress release. The tensile stresses at the top fibres of the beam were computed from the tensile strains on an elastic basis. It was found that in no case did these stresses exceed 200 psi. The strains measured at the level of the tension strand were used to determine the loss of prestress that resulted from elastic shortening of the concrete as discussed in APPENDIX B.

### 3.2.6 Test Specimens

All of the beams were of 6 x 14-5/8-in. cross-section with an effective depth of 10-in. and a total length of 12'-4". Beams A1 and B1 were tested with an 11'-0" span length and the remainder of the beams with a 10'-0" span length. All beams were loaded at two points symmetrical about midspan. Beams A1 and B1 had a constant moment region of 5'-0" and the remaining beams 4'-0". Test specimen details are shown in TABLE 3.3.

Beams A1 to A4 represented one series of beams. All of the beams in this series had a 6-in. O.D. spiral in the compression zone. The cross-section for beams of this series is shown in FIGURE 3.8(a).

TABLE 3.3

DETAILS OF TEST BEAMS

| Beam No. | $f_c'$ (psi) | Area of Reinforcement $A_s$ ($in^2$) | $P = \frac{A_s}{bd}$ | $\frac{P}{f_c'} \times 10^7$ psi | Effective Prestress ksi |
|---|---|---|---|---|---|
| A1 | 4850 | 0.4624 | 0.00770 | 15.88 | 147.0 |
| A2 | 5050 | 0.3468 | 0.00578 | 11.45 | 140.4 |
| A3 | 3220 | 0.3468 | 0.00578 | 17.95 | 130.9 |
| A4 | 3330 | 0.4624 | 0.00770 | 23.12 | 128.5 |
| B1 | 5100 | .4624 | 0.00770 | 14.00 | 137.7 |
| B2 | 4760 | .3468 | .00578 | 12.14 | 141.7 |
| B3 | 3040 | .3468 | .00578 | 19.01 | 132.6 |
| B4 | 3130 | .4624 | .00770 | 24.60 | 130.2 |
| C1 | 4890 | .4629 | .00770 | 15.75 | 138.7 |
| C2 | 4860 | .4624 | .00770 | 15.85 | 140.3 |
| C3 | 3560 | .4624 | .00770 | 21.62 | 127.6 |
| C4 | 3590 | .4624 | .00770 | 21.45 | 130.3 |

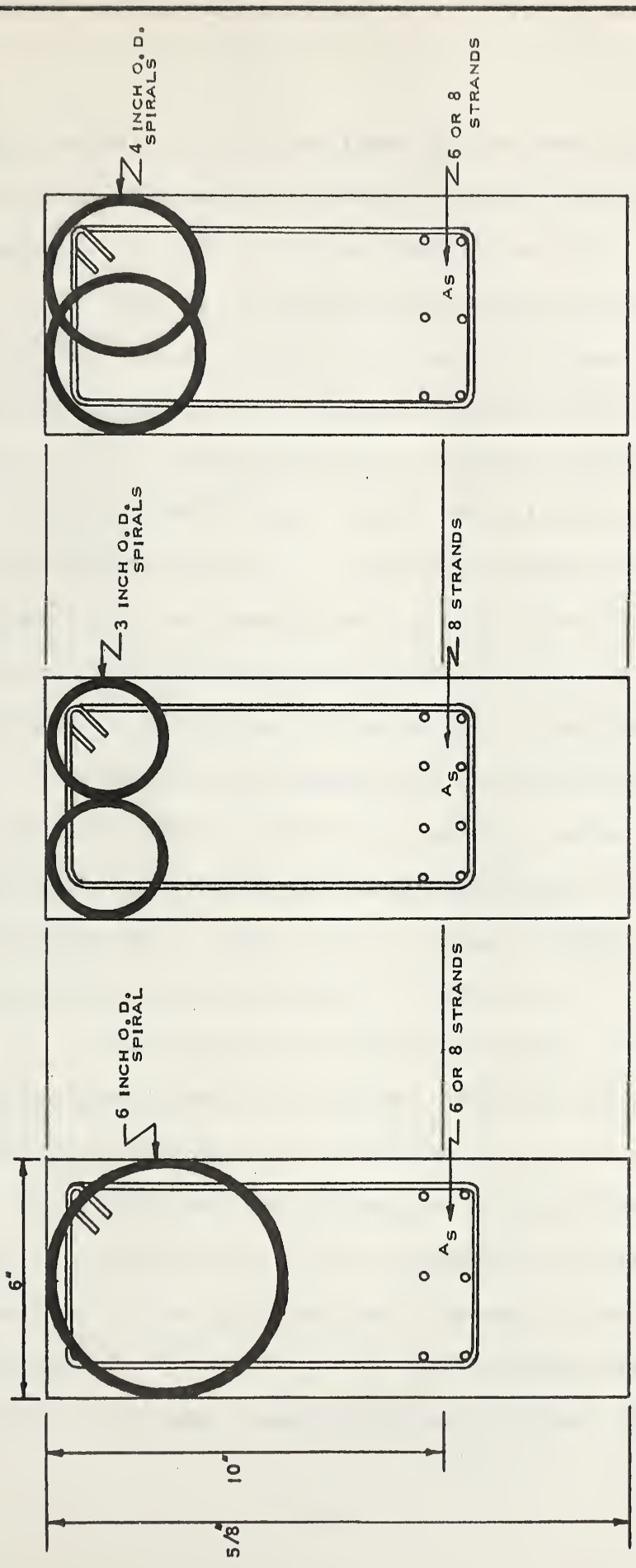


FIGURE 3.8 TEST SPECIMEN CROSS-SECTIONS

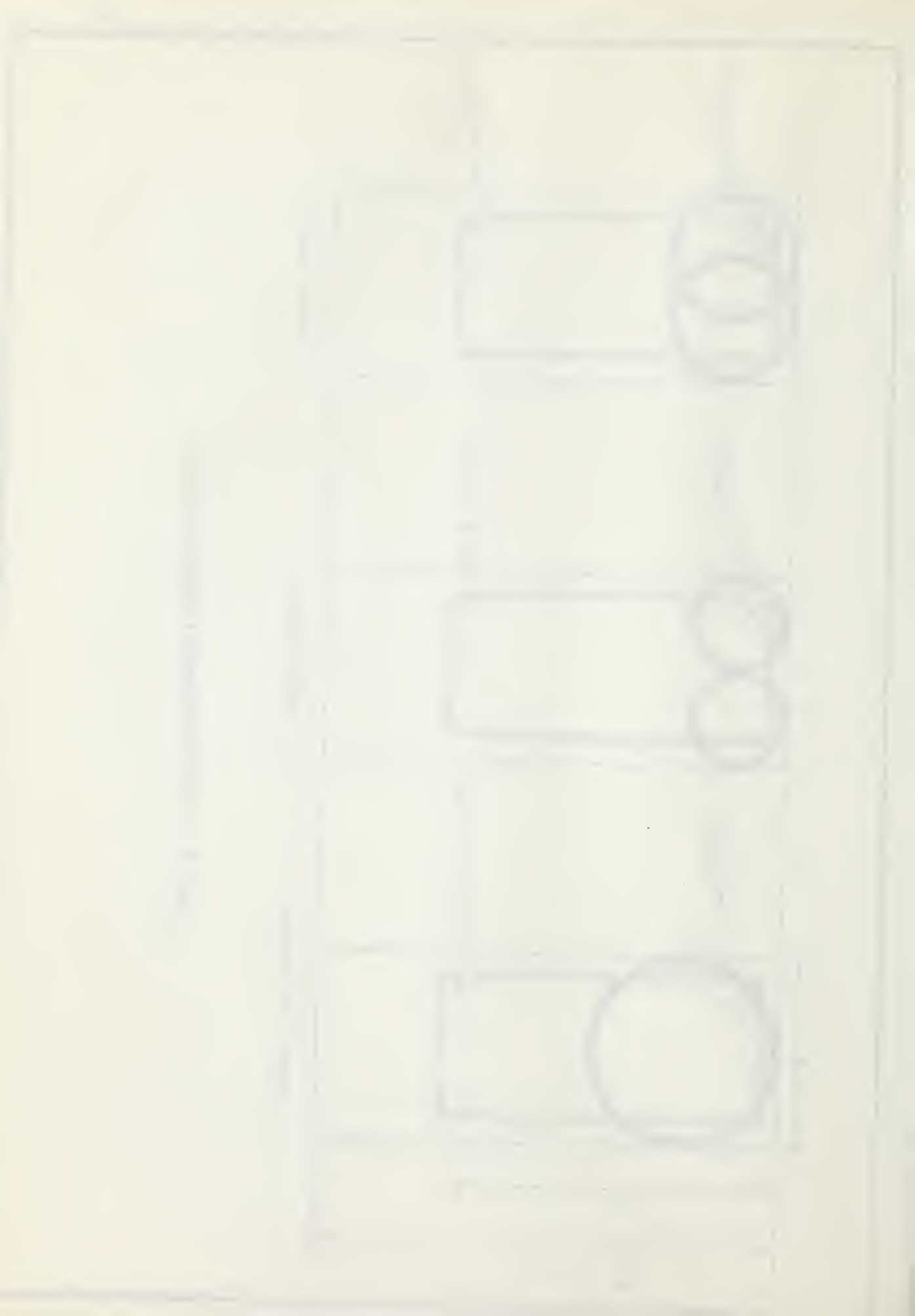

Major variables to be investigated in this series were concrete strength and amount of tension reinforcement, with effective prestress remaining constant. The spiral pitch was constant at 1-in.

Beams B1 to B4 represented another series of beams. FIGURES 3.8(b) and 3.8(c) show cross-sections of the beams of this group. Beam B1 had a cross-section as shown in FIGURE 3.8(b) with two 3-in. O.D. spirals in the compression zone. Beams B2 to B4 had two 4-in. spirals as shown in FIGURE 3.8(c). The variables in this series were the same as those used in Series A. Series A and Series B beams were cast concurrently, in that beam A1 was cast with B1, A2 with B2 and so on. The two series were therefore easily combined into one overall series to study the effects of variation in type of spiral confinement.

Beams C1 to C4 constituted a third series having as variables concrete strength and spiral pitch with percentage of tension reinforcement and effective prestress remaining constant. All of the beams of this series had a cross-section as shown in FIGURE 3.8(a). For both high and low concrete strengths a spiral pitch of 2 and 3-in. was used.

The spirals in all beams were placed in the regions of the top and side surfaces of the beams, therefore representing the condition of minimum shell outside the confined core of the spirals. It was impossible to obtain this condition perfectly at the top of the beam due to the settling of the spiral caused by the immersion type vibrator. As a result some cover on the spiral existed. However, in no case did this cover exceed 3/8-in. The spirals in all beams extended over seven feet and were placed in the beams symmetrically about midspan. Details of spiral rein-

forcement are shown in TABLE 3.4.

All shear reinforcement was designed on the basis of ACI 318-63 (11) and then nominally increased to handle the higher shears that would result from increasing the final failure moment because of confinement of the concrete in the compression zone. Details of shear reinforcement are shown in TABLE 3.5.

## 3.3 Testing Procedures

### 3.3.1 Instrumentation

The instrumentation used on the test beams is shown in FIGURE 3.9.

The distribution of strains over the depth of the beam was measured with an 8-in. Demec deformation gage. Five gage lines were used on all beams except for beam A4 which had an additional gage line 3-in. from the top of the beam. Gage columns 1 to 8 inclusively were used during tests of beam A1 and B1. The remaining beam were tested measuring strains across gage columns 2 to 7 inclusively. A gage line on the top of each beam which was used to record tensile strains at transfer of prestress could not be read during the beam test since it was below the distributing beam. The steel Demec points were 1/4-in. in diameter. Sealing wax was used to fasten the points to the beams.

Type A3 SR-4 electrical resistance strain gages were mounted on the top of all beams. They were located on the longitudinal centerline of the beams on one side of midspan at distances of 3, 9 and 18-in. as shown in FIGURE 3.9. Type A7 SR-4 strain gages were mounted on the spirals at the top and side of the same loop in any one spiral. These gages were used to indicate relative magnitude of spiral strains and to indicate to

TABLE 3.4

DETAILS OF SPIRAL REINFORCEMENT

| Beam No. | Bar Size | Outside Diameter | Number of Spirals | Spiral Pitch | Lateral Binding Ratio ($P_b$) |
|---|---|---|---|---|---|
| A1 | #2 | 6" | 1 | 1" | .0347 |
| A2 | #2 | 6" | 1 | 1" | .0347 |
| A3 | #2 | 6" | 1 | 1" | .0347 |
| A4 | #2 | 6" | 1 | 1" | .0347 |
| B1 | #2 | 3" | 2 | 1" | .0694 |
| B2 | #2 | 4" | 2 | 1" | .0737 |
| B3 | #2 | 4" | 2 | 1" | .0737 |
| B4 | #2 | 4" | 2 | 1" | .0737 |
| C1 | #2 | 6" | 1 | 3" | .0116 |
| C2 | #2 | 6" | 1 | 2" | .0174 |
| C3 | #2 | 6" | 1 | 3" | .0116 |
| C4 | #2 | 6" | 1 | 2" | .0174 |

TABLE 3.5

DETAILS OF SHEAR REINFORCEMENT

| Beam No. | Bar Size | Spacing |
|---|---|---|
| A1 | #2 | 4" |
| A2 | #3 | 6" |
| A3 | #3 | 6" |
| A4 | #3 | 6" |
| B1 | #2 | 4" |
| B2 | #3 | 6" |
| B3 | #3 | 6" |
| B4 | #3 | 6" |
| C1 | #3 | 5" |
| C2 | #3 | 5" |
| C3 | #3 | 5" |
| C4 | #3 | 5" |

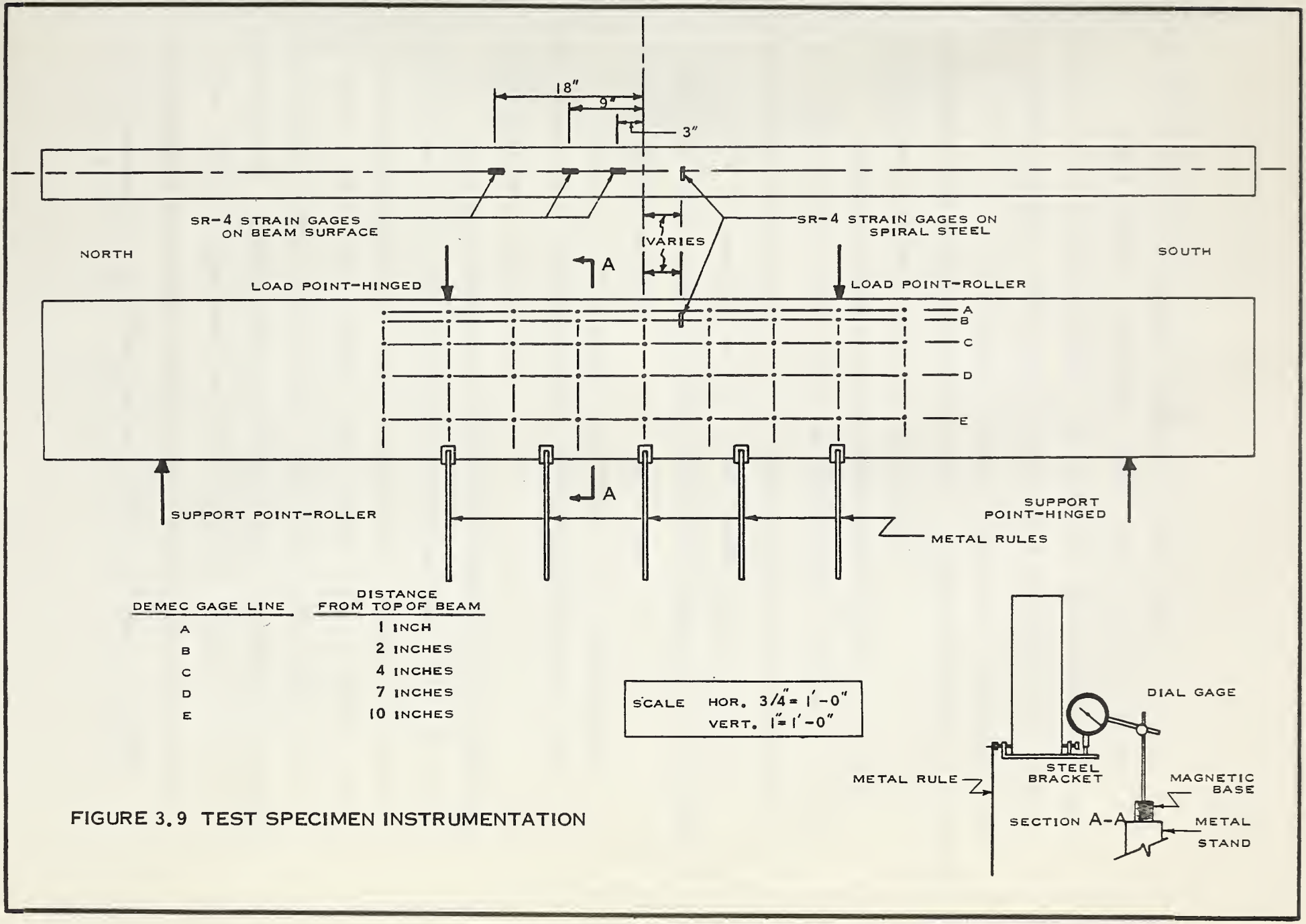


FIGURE 3.9 TEST SPECIMEN INSTRUMENTATION

some degree the distribution of stress around the spiral.

The electrical resistance strain gages on the concrete were mounted in the following manner: the surface was first ground smooth with a portable grinder, a thin coat of shellac was next applied and allowed to dry resulting in a sealed smooth surface; the electrical resistance strain gages were then attached to the beam using a Budd GA-1 Cement Kit in accordance with the manufacturer's recommended procedures.

Electrical resistance strain gages were mounted on the spiral in a similar manner. The concrete was chipped clear to expose the spiral for a length of about 1-1/2-in. The steel was then rubbed clean with emery cloth. The surface was then further cleaned using the Budd GA-1 cleaner and the gages attached using the Budd GA-1 Cement Kit in accordance with recommended procedures.

Strains in the concrete were measured with a Baldwin-Lima-Hamilton electrical strain indicator and strains in the spiral with a Budd electrical strain indicator.

Dial gages were used to measure beam deflections up to spalling. They were mounted in an inverted position and supported by magnetic bases on a rigid metal frame. Dial gages were placed at midspan, at the load points and midway between midspan and the load points. Deflections were also recorded using a precise level. Steel rules at the front face of the beam were suspended from the prepared brackets on which the dial gages rested. The dial gages were removed at spalling to prevent them from being damaged, and further deflections were read with the level. Dial gage arrangement and steel rule support details are shown in FIGURES

3.9 and 3.10

3.3.2 Loading Apparatus

Two 44 kip Amsler hydraulic jacks were used to load the beams. The loading frame and jacking arrangement details are shown in FIGURES 3.11 and 3.12. An Amsler Pendulum Dynamometer was used to measure applied jack loads. A load maintainer built into the system made it possible to maintain the load at a constant level, independent of the rate of creep which occurred at any applied load.

Load was applied to the test beam through a distributing beam. The distributing beam was used only to maintain proper distance between the jacks during loading. The jacks were positioned directly above the test beam load points and therefore introduced no flexural bending into the distributing beam. Load was transferred from the distributing beam to the test beam through a roller and grooved bearing plates at one end and a roller and flat bearing plates at the other end. The locations of hinged and roller type supports used in the loading apparatus are shown in FIGURE 3.9. To provide an even stress distribution all bearing plates were attached to the concrete with Plaster of Paris.

3.3.3 Testing Procedure

Before any application of load, initial readings of strain gages, Demec gage lines, deflection dial gages and precise level were taken. An average of 12 load increments were applied before failure. In most cases three increments of load were applied before cracking. The load increment was reduced for continued loading after initial flexural cracking and further reduced for loading beyond initial compression zone spalling.

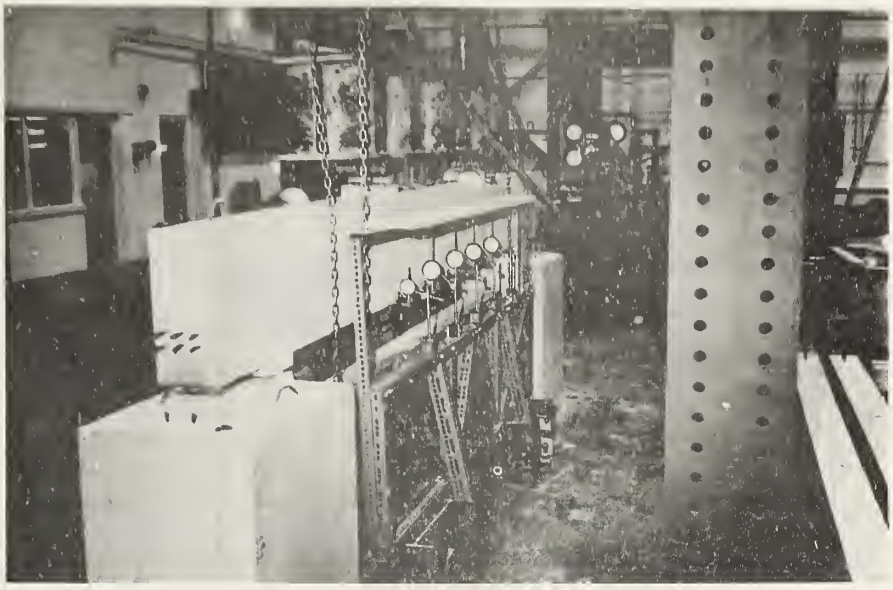

FIGURE 3.10 DIAL GAGE ARRANGEMENT

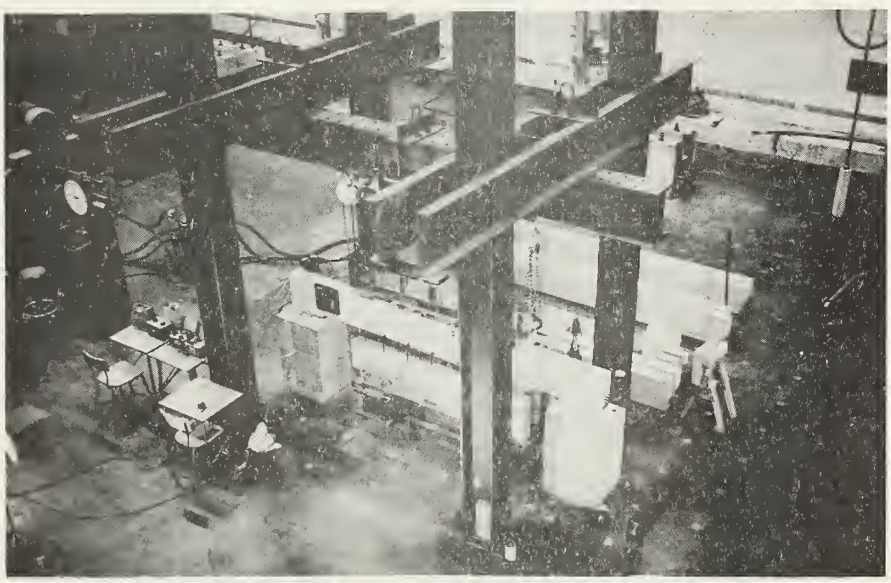

FIGURE 3.11 INSTRUMENTATION AND
TEST APPARATUS

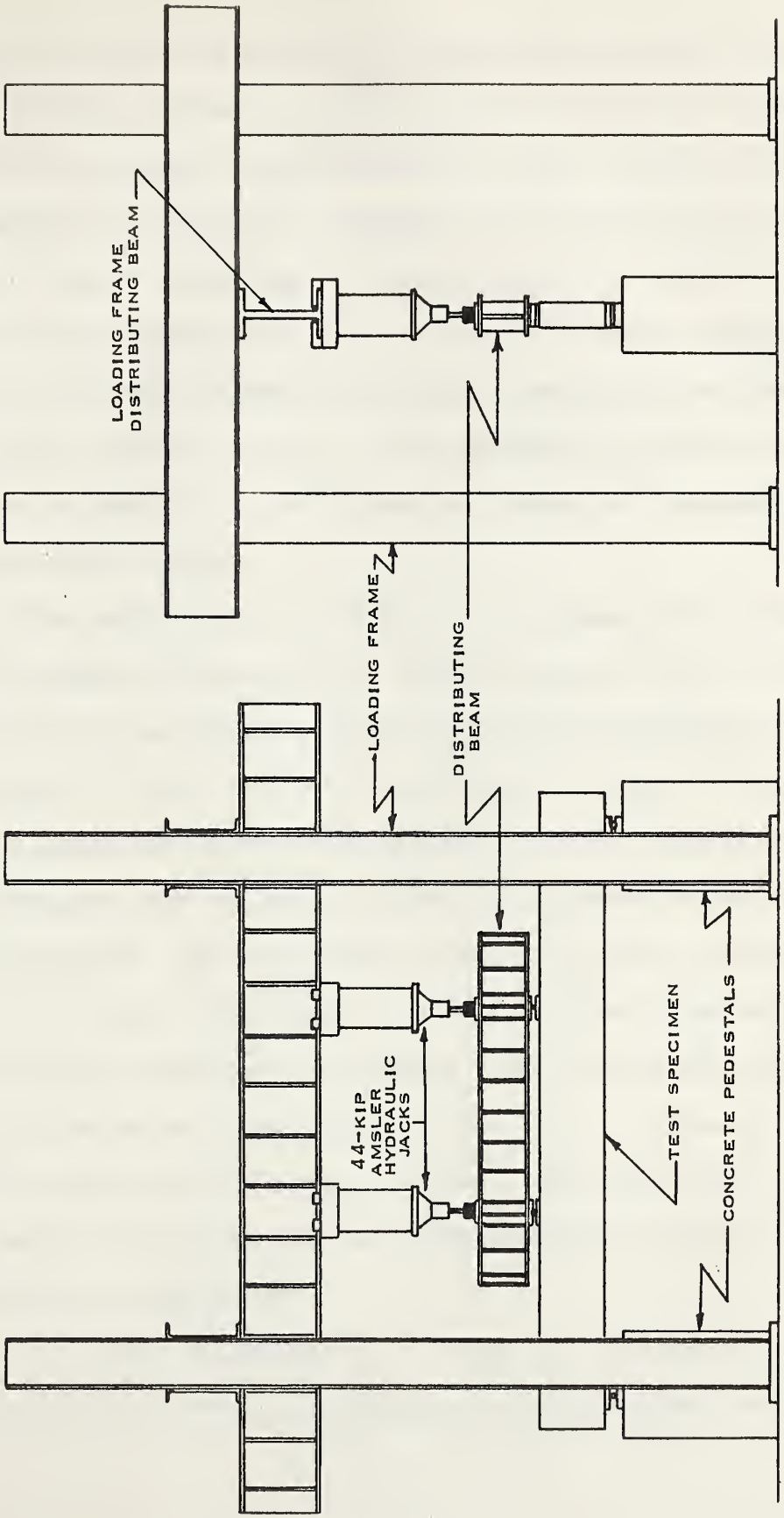


FIGURE 3.12 LOADING FRAME ARRANGEMENT

When the predicted spalling load was approached, the Amsler Dynamometer dial was observed carefully in order that the peak load just before spalling could be observed. An attempt was then made to adjust the applied load immediately to the level to which the dial needle dropped upon spalling. This procedure made it possible to take a complete set of data at the stage immediately after spalling. In tests on beams with the smaller spirals, the amount of concrete spalling off was small and spalling was a gradual process. It was impossible to obtain any peak load prior to spalling in these tests and loading was continued to the next even load increment.

The deflections in the majority of the beams were excessive. Since the maximum extension of the Amsler jacks was 5-in., it was necessary to provide some form of restraint to hold the loaded beam in a deflected position while jacks were being reset and plates introduced between the jacks and the distributing beam. A 1/2-in. wall, 4-in. diameter pipe column, with 6-in. square, 1-1/2-in. milled plates welded to each end, was prepared. The total length of the pipe column was 40-in. as compared to a closed jack height of 36-in. The pipe column was inserted between the distributing and the loading frame distributing beam at midspan when a jack extension slightly greater than 4-in. was observed. The jacks were then contracted transferring the load to the pipe column. The introduction of plates under the jack heads allowed an additional 5-in. of deflection at the load points.

The order of reading and recording data throughout a beam test was the same for all tests. Instrumentation readings were taken in the

following order:

(a) dial gages (level, after spalling)

(b) demec gage readings (not taken at loads near failure)

(c) electrical strain gages

(d) level

(e) dial gages (up to spalling).

Crack patterns were marked while the above readings were being taken and in some cases photographs were taken at intermediate loads. The beams were loaded until total collapse or in cases of unbonding, until large deflections occurred at constant load. Photographs were taken at the completion of the tests to record crack patterns and the modes of failure.

# CHAPTER IV

# PRESENTATION OF TEST RESULTS

## 4.1 Load-Deflection Relationships

Beam deflections were measured with dial gages located at midspan, the load points and midway between midspan and the load points. These dial gages were removed at spalling to avoid damaging them and further deflections were measured with a precise level trained on steel rules suspended from the beam and located at the same positions as the dial gages.

Deflections were read immediately after application of the load. At higher constant sustained loads, where creep was more pronounced, deflection readings were also obtained just prior to increasing the load. All deflections were measured relative to the initial cambered position of the beams.

Load-midspan deflection curves for all beams are shown in FIGURES 4.1 to 4.6.

## 4.2 Strain Distribution over the Depth of the Beams

Strain distributions over the depth of the beams were obtained by measuring the deformations across the columns on each horizontal gage line with an 8-in. Demec gage. All beams, except Beam A4, had five gage lines at different elevations over the depth of the beam. Beam A4 had six gage lines. The top three gage lines for all beams were so located

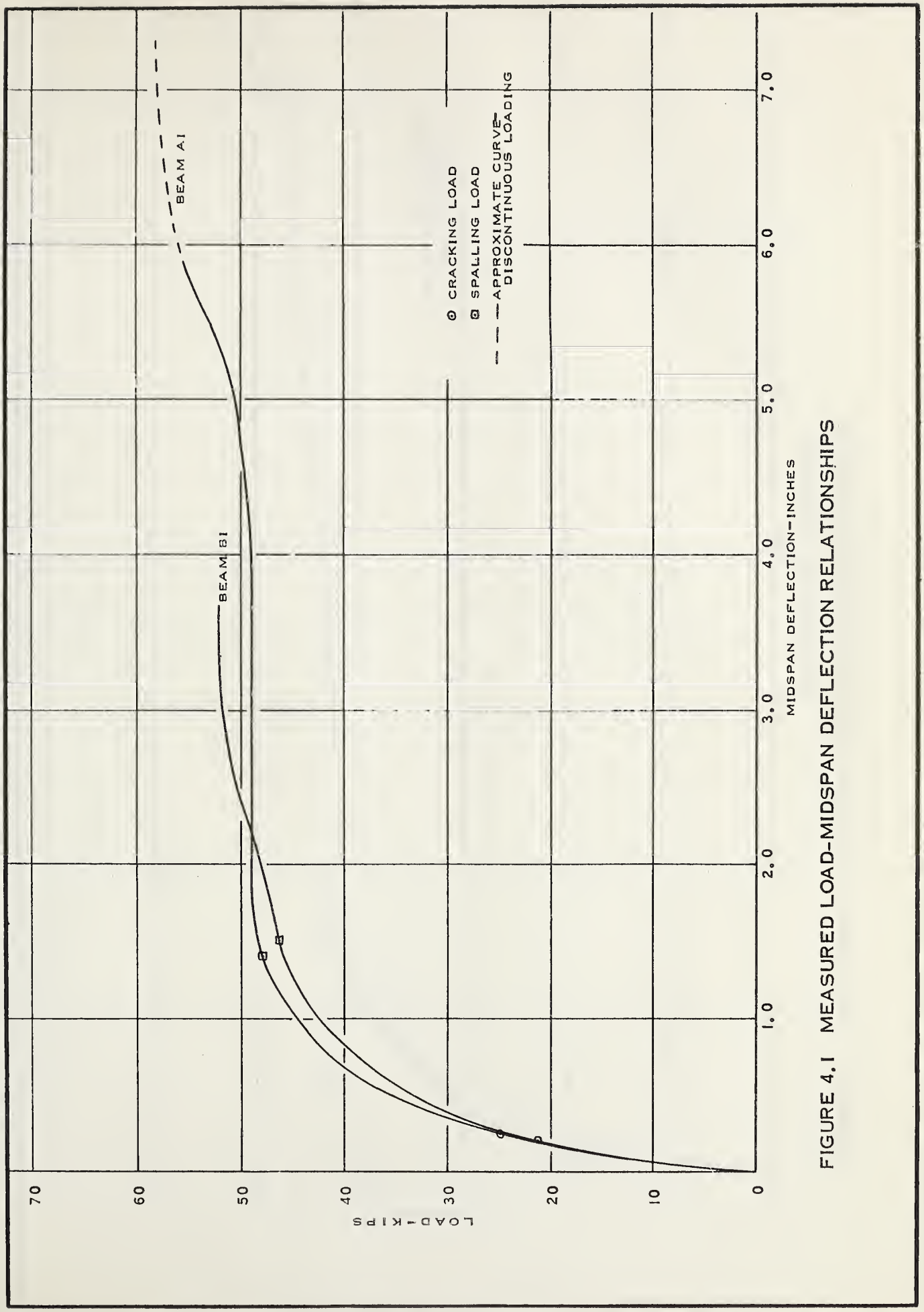


FIGURE 4.1 MEASURED LOAD-MIDSPAN DEFLECTION RELATIONSHIPS

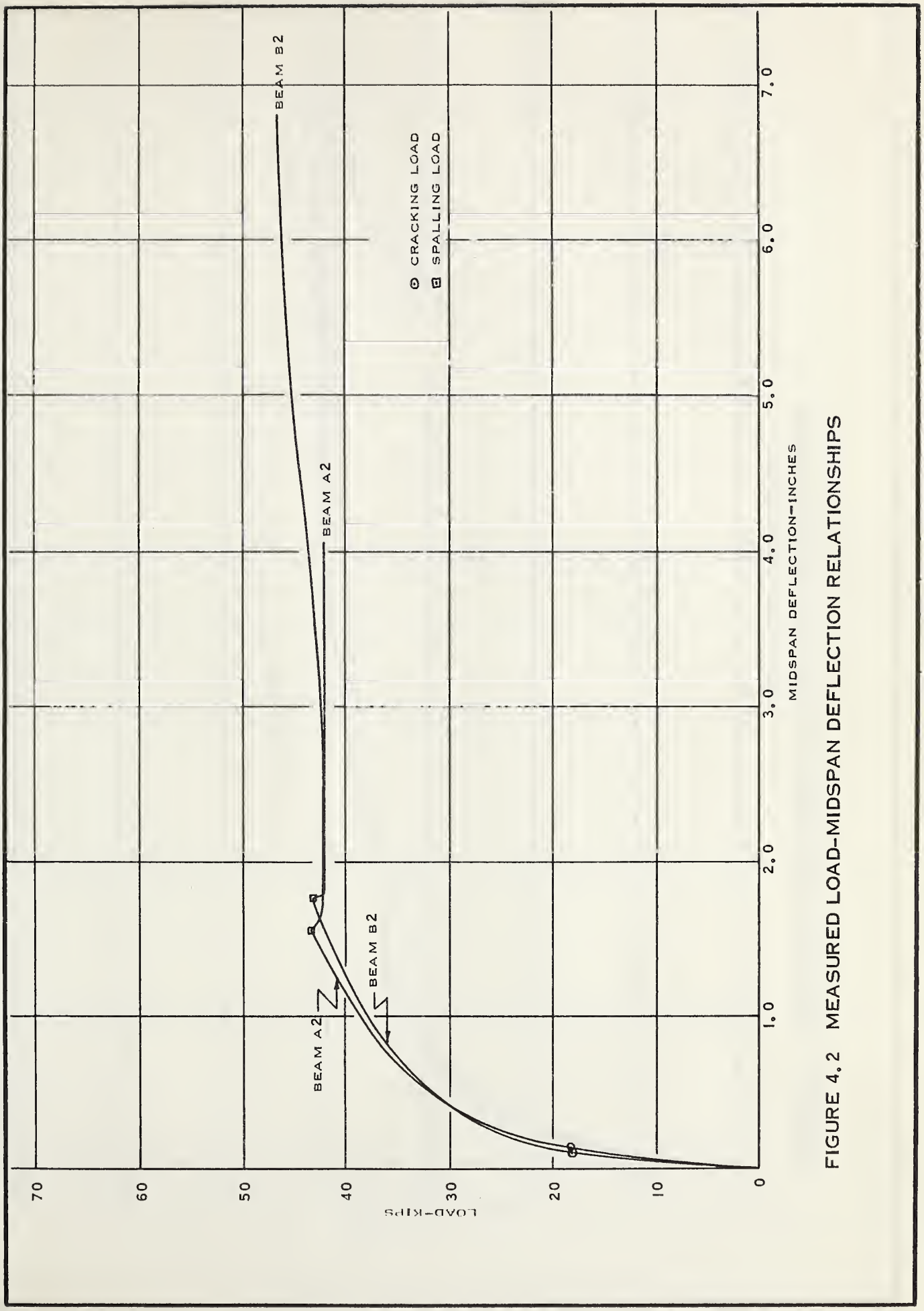


FIGURE 4.2 MEASURED LOAD-MIDSPAN DEFLECTION RELATIONSHIPS

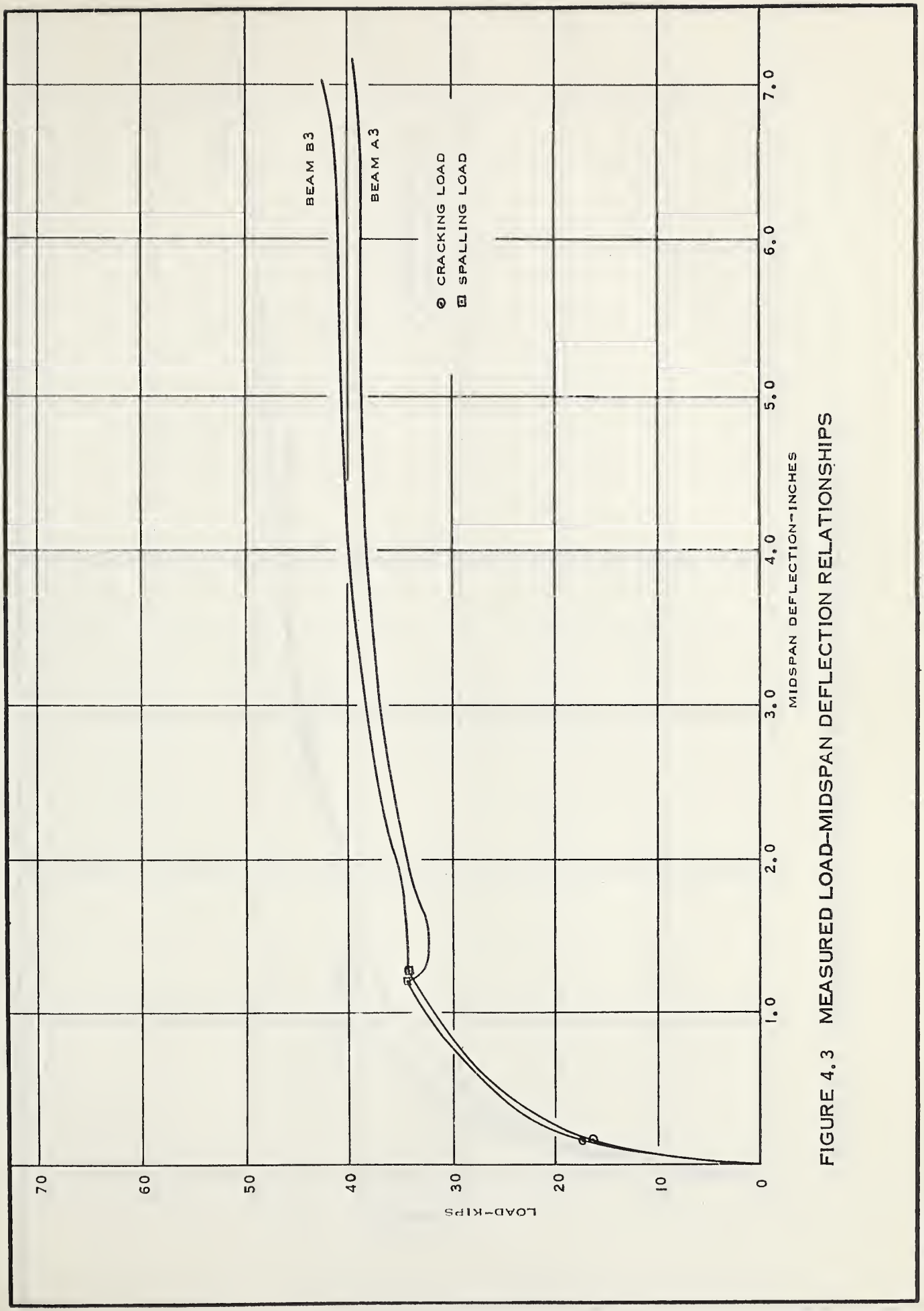


FIGURE 4.3 MEASURED LOAD-MIDSPAN DEFLECTION RELATIONSHIPS

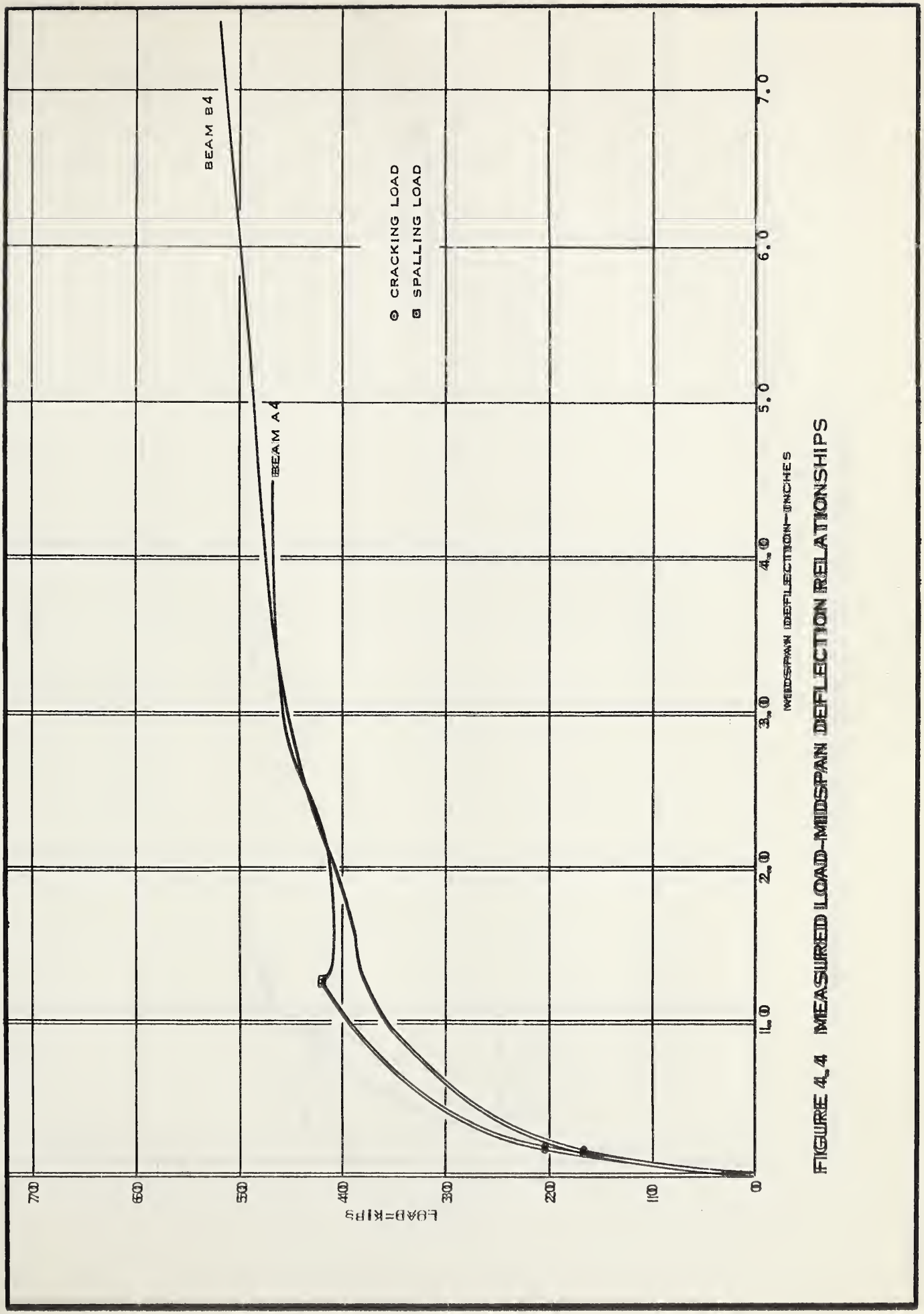


FIGURE 4.4 MEASURED LOAD-MIDSPAN DEFLECTION RELATIONSHIPS

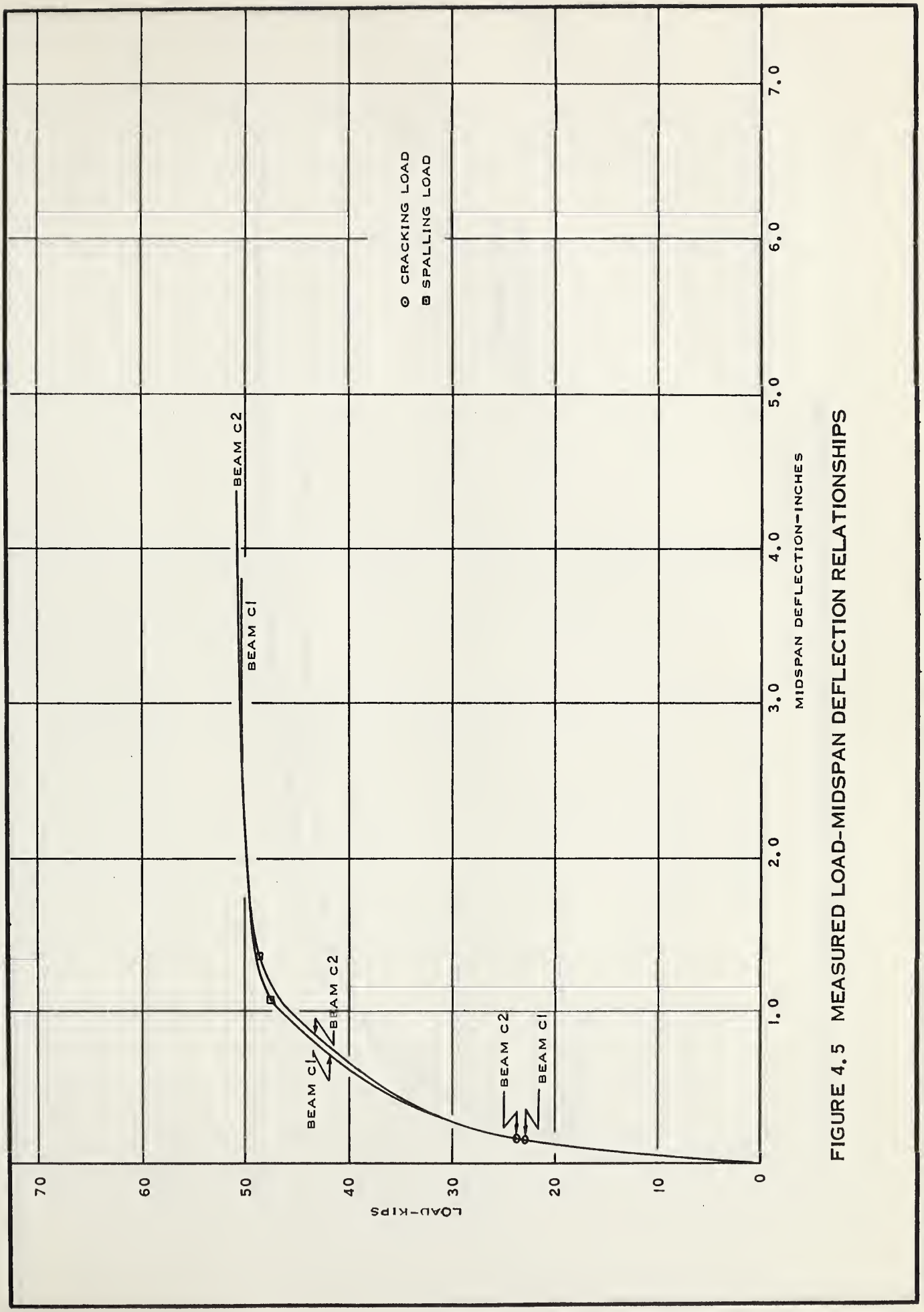


FIGURE 4.5 MEASURED LOAD-MIDSPAN DEFLECTION RELATIONSHIPS

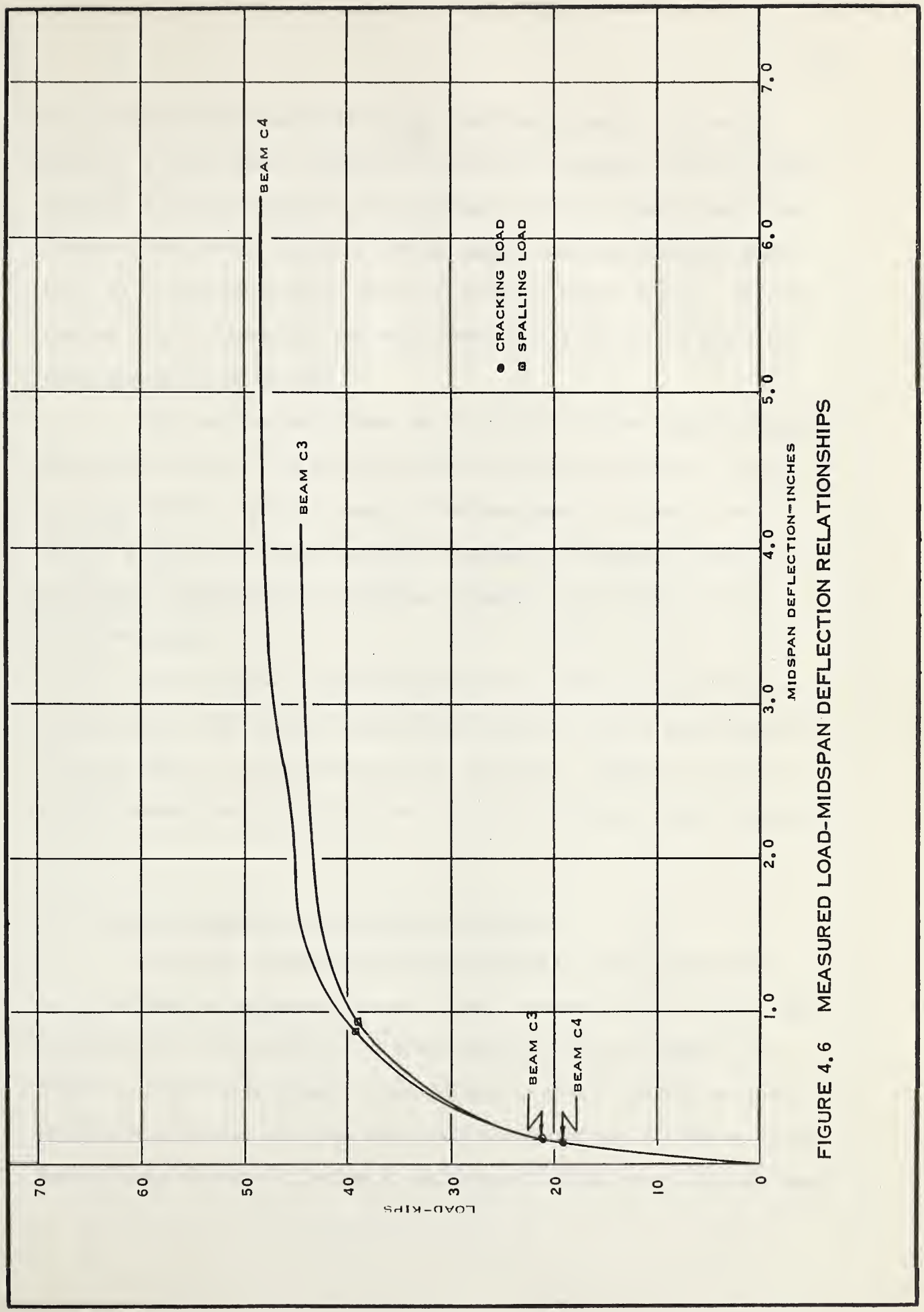


FIGURE 4.6 MEASURED LOAD-MIDSPAN DEFLECTION RELATIONSHIPS

that they would be essentially in the compression zone. The two top gage lines were always completely destroyed at spalling. The extra gage line was included on Beam A4 in an attempt to have an intact gage line closer to the area of spalling. Eight gage columns were used on Beams A1 to B1 to instrument fully the 5-ft. constant moment region. This was reduced to six columns for the other beams tested since they had a constant moment region of 4-ft.

For various load levels up to cracking strains along each gage line were similar. Once cracking had occurred the strains on a particular gage line varied over the length of the beam since the strains were largely a function of crack opening as opposed to concrete deformations. The strains recorded were, therefore, dependent on the crack pattern which developed.

In the region of constant moment the average strain distribution for the entire instrumented region was found to be linear and therefore could be used for the determination of curvatures. FIGURE 4.7 shows a typical average strain distribution obtained at various levels of increasing load.

## 4.3 Strains on the Top of the Beams at Spalling

All of the beams tested were designed to fail in compression in the absence of confined concrete in the compression zone. Since confining spirals were present, the beams actually failed at higher load levels. In the later stages of loading the concrete outside the spirals spalled off, whereas the concrete within the spiral was further stressed. During tests of beams of Series A and Series B, which eventually collapsed

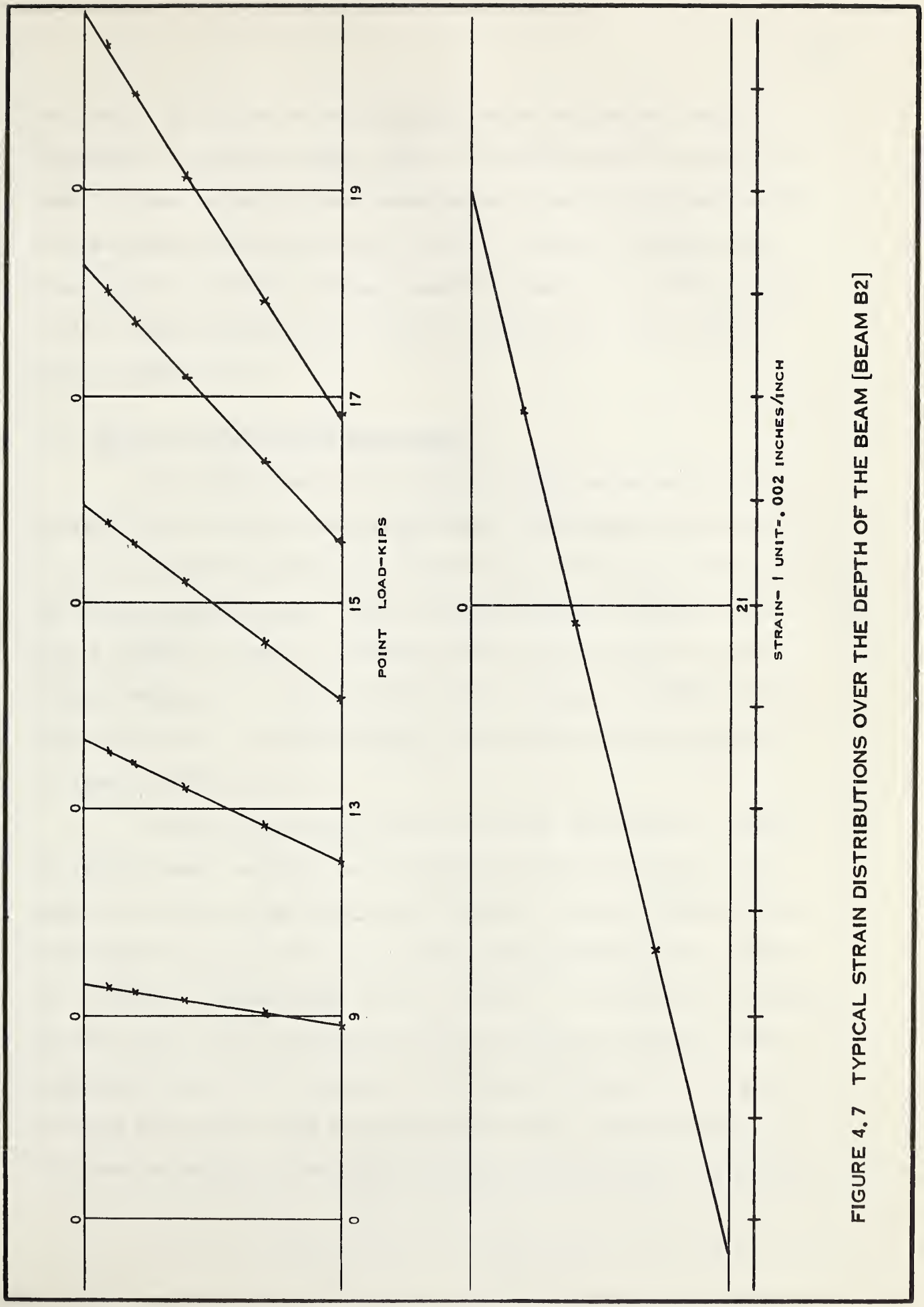


FIGURE 4.7 TYPICAL STRAIN DISTRIBUTIONS OVER THE DEPTH OF THE BEAM [BEAM B2]

as a result of failure in tension, spalling was uniform and complete throughout the constant moment region. The spalling which occurred in tests of beams in Series C was concentrated at various locations in the constant moment region and had not occurred uniformly throughout this region prior to failure. Average concrete strains in the extreme upper fibres at spalling were of the order of 0.004 in./in. with values as high as 0.006 in./in.

## 4.4 Strains in the Spiral Reinforcement

Two A7 SR-4 electrical resistance strain gages were used to measure strains in the spiral reinforcement. The gages were attached to the top and side surfaces of a single loop of the spiral located in the constant moment region. Spiral strains recorded in Series A and Series B beams are shown in FIGURES 4.8 and 4.9 as a function of beam midspan deflection. A similar relationship is given in FIGURE 4.10 for beams of Series C. A typical spiral strain-versus-load relationship is shown in FIGURE 4.11.

In some cases spiral strains could not be measured at stages of loading beyond spalling due to loosening of the electrical strain gages as a result of spalling of the concrete. For those cases in which the side strain gages were intact after spalling, readings were obtained up to the last load increment prior to failure. In several of the beams strains at the top of the spirals were measured up to failure. Where yielding occurred in the spirals, as in beams of Series C, the highest level of strain that could be measured was that at initial yielding. The rate of increase of strain after initial yielding was so great that

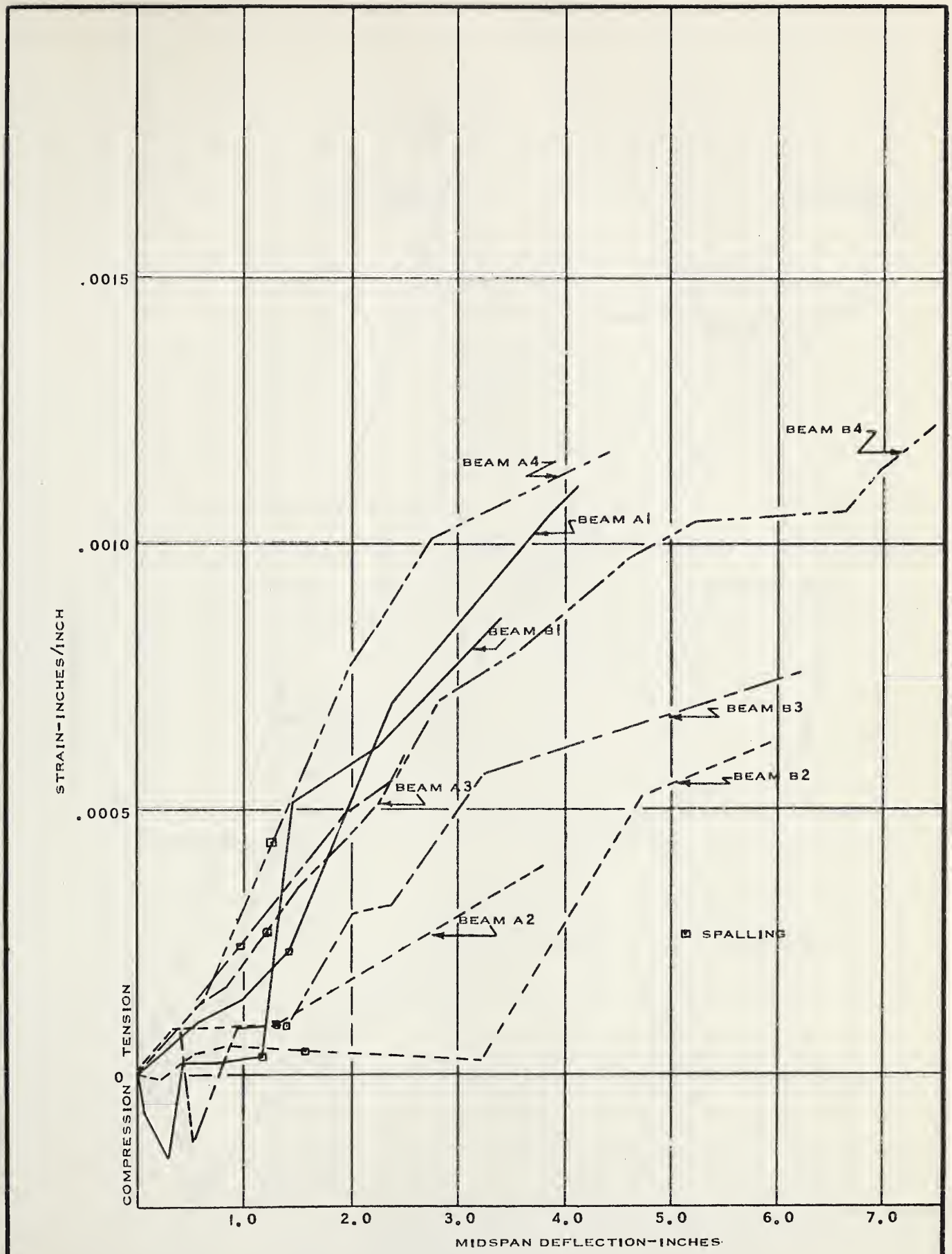


FIGURE 4.8 SPIRAL STRAINS VERSUS BEAM MIDSPAN DEFLECTIONS [SIDE STRAIN GAGE]

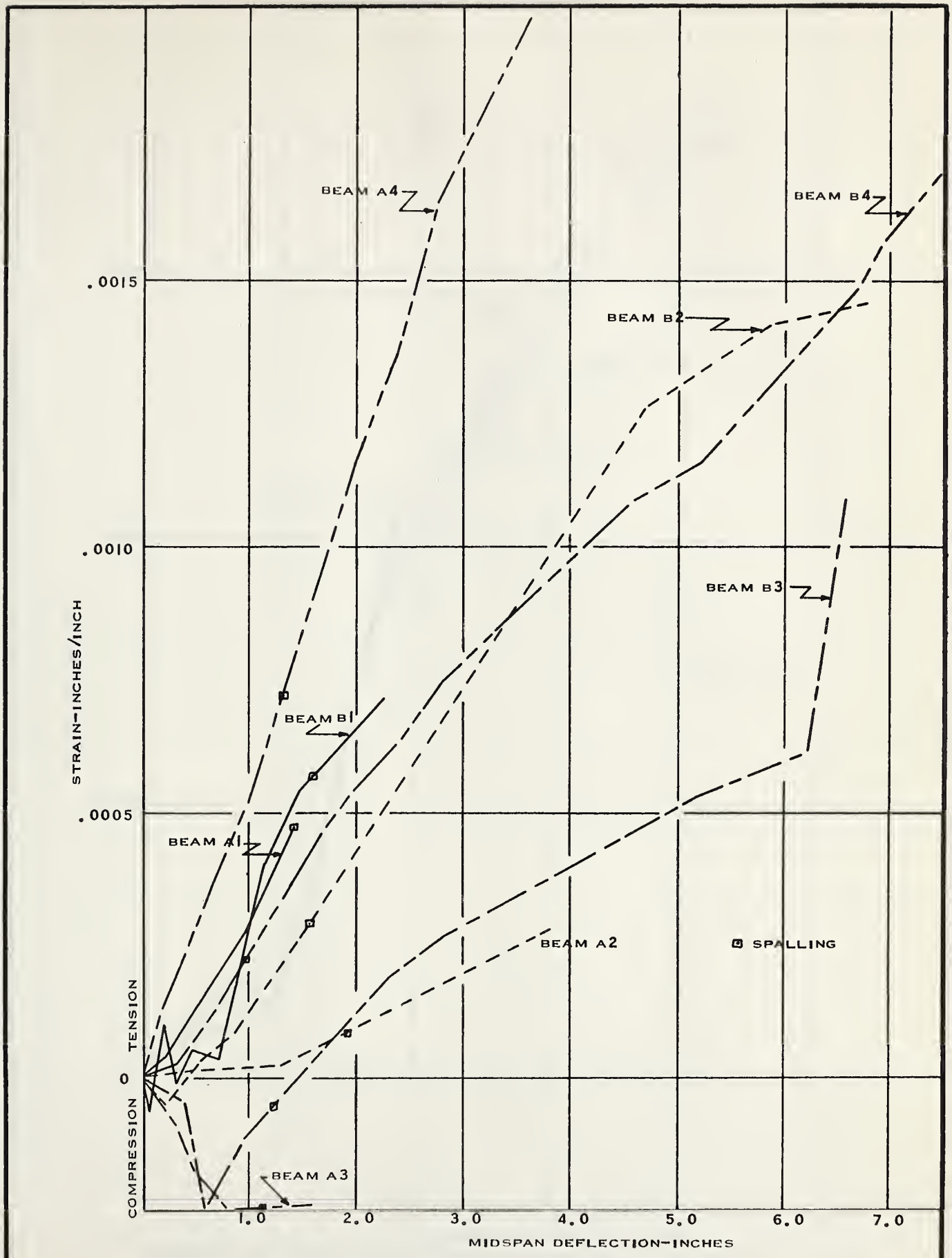


FIGURE 4.9 SPIRAL STRAINS VERSUS BEAM MIDSPAN DEFLECTIONS [TOP STRAIN GAGE]

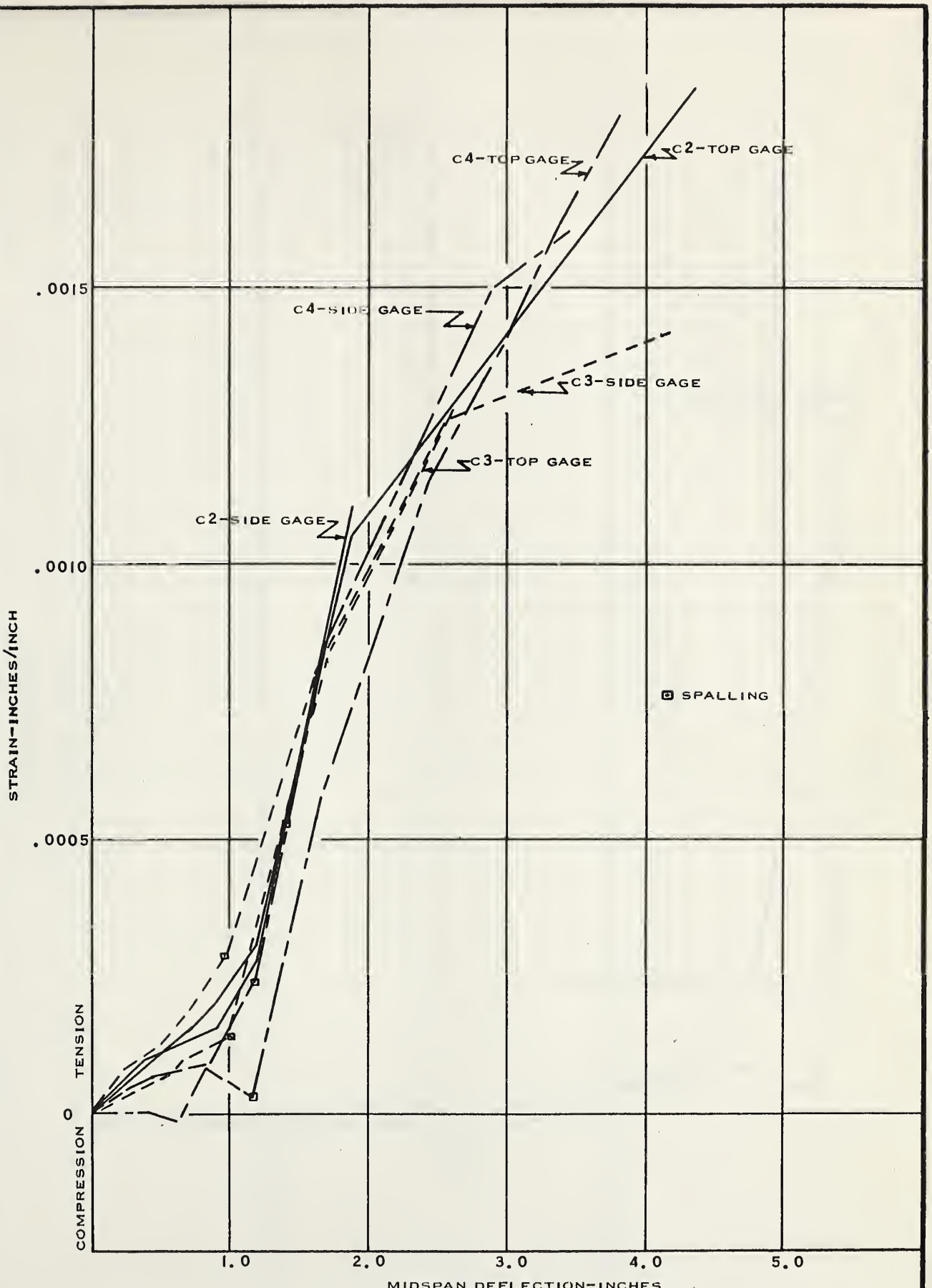


FIGURE 4.10 SPIRAL STRAINS VERSUS BEAM MIDSPAN DEFLECTIONS

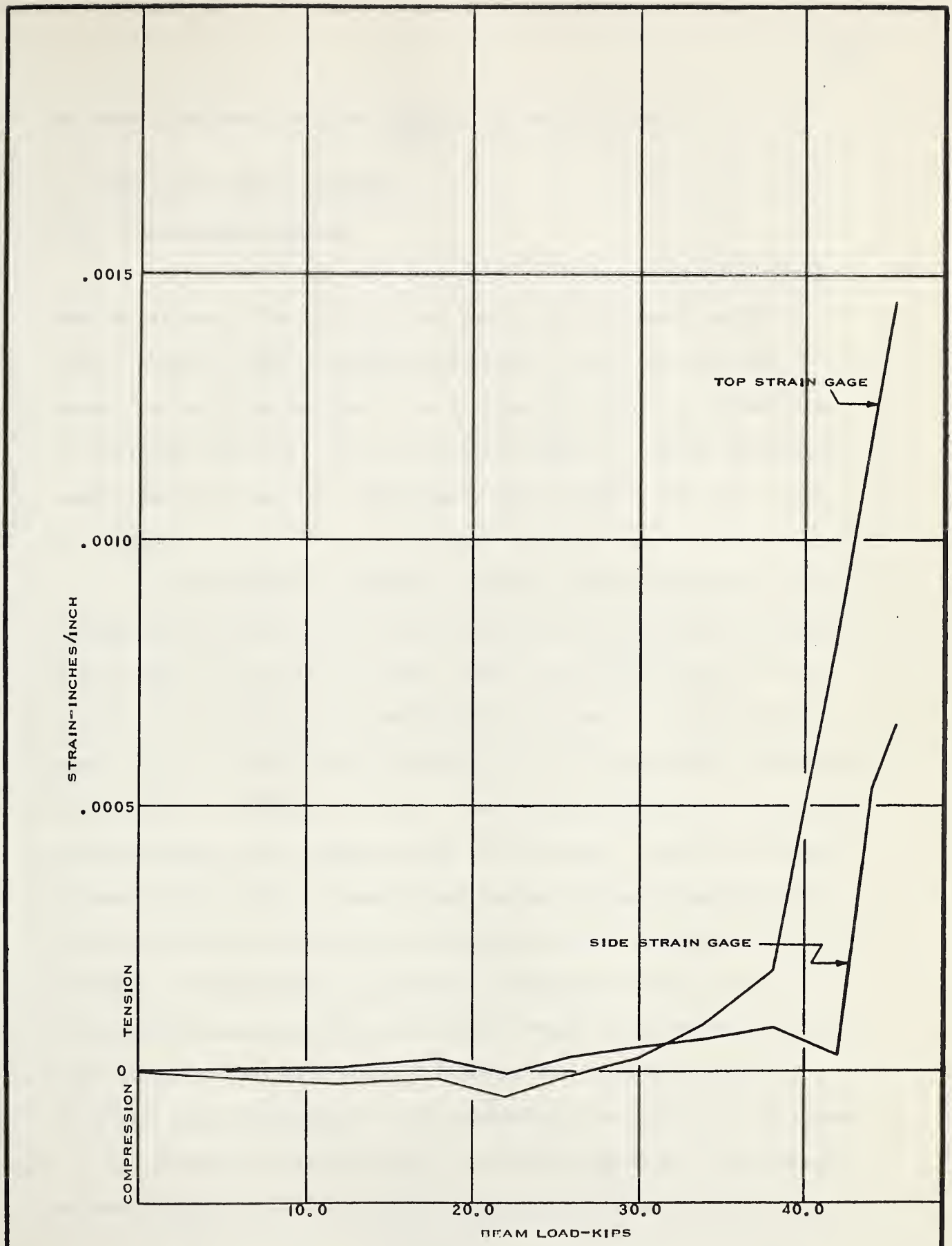


FIGURE 4.11 SPIRAL STRAINS VERSUS BEAM LOAD [BEAM B2]

the strain indicator could no longer be balanced and read.

## 4.5 Behavior of Test Specimens

### 4.5.1 Introductory Remarks

All of the beams were over-reinforced with respect to normal tension failures. The strain in the tension reinforcement was still elastic when the limiting compressive strains in the concrete were reached and spalling occurred. The discussion of behavior presented in the following sections will not necessarily apply to similar beams with lesser amounts of tension reinforcement since yielding can occur prior to spalling.

The response of a member to load is best illustrated by load-deformation characteristics, which show both the strength and ductility of the member. Since all the beams tested were bonded beams with the same level of prestress, the behavior for each beam was generally the same. This is evident from the similarity of the load-midspan deflection curves shown in FIGURES 4.1 to 4.6. Four distinct stages were indicated, each represented by a change in slope of the curves. The major factors influencing the extent of these stages during loading to failure were: the stress-strain relationships of the concrete and the steel, the amount of tension reinforcement, the degree of confinement of the concrete in the compression zone and the span length. Observations made during the tests indicated that each stage of behavior was related to different particular stress conditions in the concrete and the tension reinforcement.

The first stage of behavior is that in which the concrete and the steel strains are elastic and is represented by the initial linear

portion of the load-deflection curve. The second stage showed an increased rate of deflection with load after initial flexural cracking. The steel was still elastic in this stage, as discussed previously in this section. The third stage was initiated at spalling. It was represented by a sudden reduction in beam stiffness and a subsequent redistribution of stresses in the compression zone as the concrete displaced laterally and gained restraint from the confining spiral. The concrete acted plastically in this stage while the tension steel was still elastic. Large deflection occurred at constant load until the equilibrium that formerly existed between the rectangular compressed concrete and the tension reinforcement prior to spalling was obtained between the confined concrete and the tension steel. The fourth stage corresponded to an inelastic stress condition in the steel. Since this portion of the load-deflection diagram reflected the stress-strain relationship of the tension steel, it was nearly flat. A typical load-midspan deflection curve is shown in FIGURE 4.12, CURVE A.

### 4.5.2 The First Stage of Behavior

The first stage of behavior was represented by the initial linear portion of the load-deflection diagram and terminated at the first formation of flexural cracks. The extent of this first stage was dependent on the level of prestress, the amount of tension reinforcement, the eccentricity of the prestressing force and the modulus of rupture for the concrete. It can be seen from the load-deflection curves that the cracking moment was higher for the more heavily reinforced beams. This was a result of the higher prestressing force which produced higher

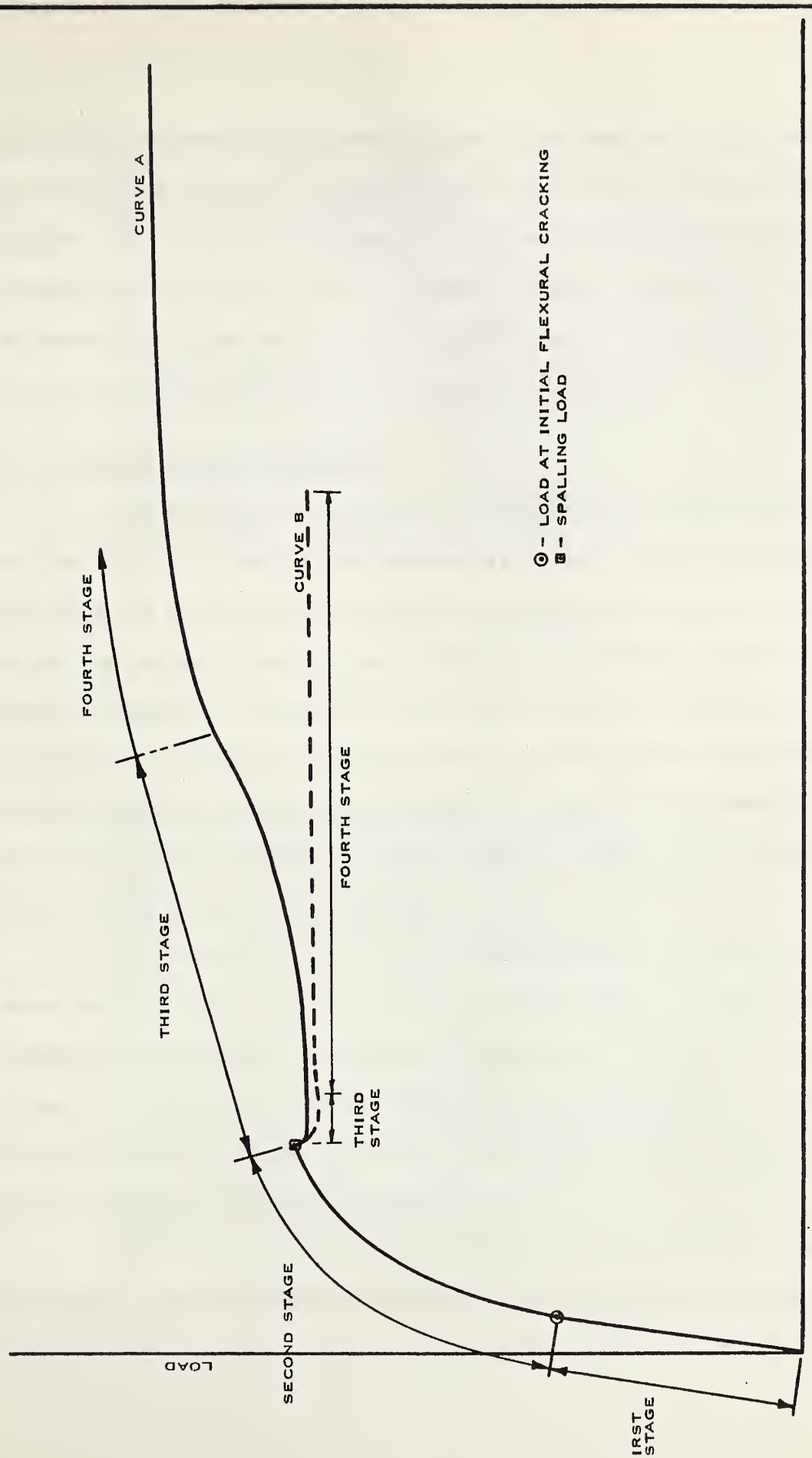


FIGURE 4.12 TYPICAL LOAD-MIDSPAN DEFLECTION RELATIONSHIP FOR A BEAM WITH CONFINED CONCRETE

compressive stresses in the lower fibres of the beam at initial conditions. This force had to be overcome before the bottom fibres were placed in tension. The cracking moment was also higher for beams with higher strength concrete as a result of a higher modulus of rupture. The influence of the presence of spiral reinforcement in the compression zone is negligible during the first stage of behavior.

### 4.5.3 Second Stage of Behavior

The second stage of behavior commenced with the formation of vertical cracks in the constant moment region and ended at spalling. The number of vertical flexural cracks increased as the load was increased beyond the initial cracking load. Typical crack patterns observed are shown in FIGURES 4.13 and 4.14. From these figures it can be seen that the flexural cracks rose rapidly at first cracking and as loading was continued crack extensions were reduced for additional increments of load. At later stages of loading the cracks began to "fork" out. Inclined cracks in the shear span also began to form.

The change in slope of the load-deflection curves was, for all beams, small at first cracking since the large amount of tension reinforcement was capable of sustaining the additional tensile force transferred to it from the concrete with little increase in stress. This resulted in only a slight increase in steel strain and, consequently, a small increase in beam midspan deflection.

The rate of change of deflection with load increased after cracking. The progressive reduction in beam stiffness was caused by movement of the neutral axis in an upwards direction as a result of


FIGURE 4.13 CRACK PATTERN OF A BEAM
FAILING IN TENSION

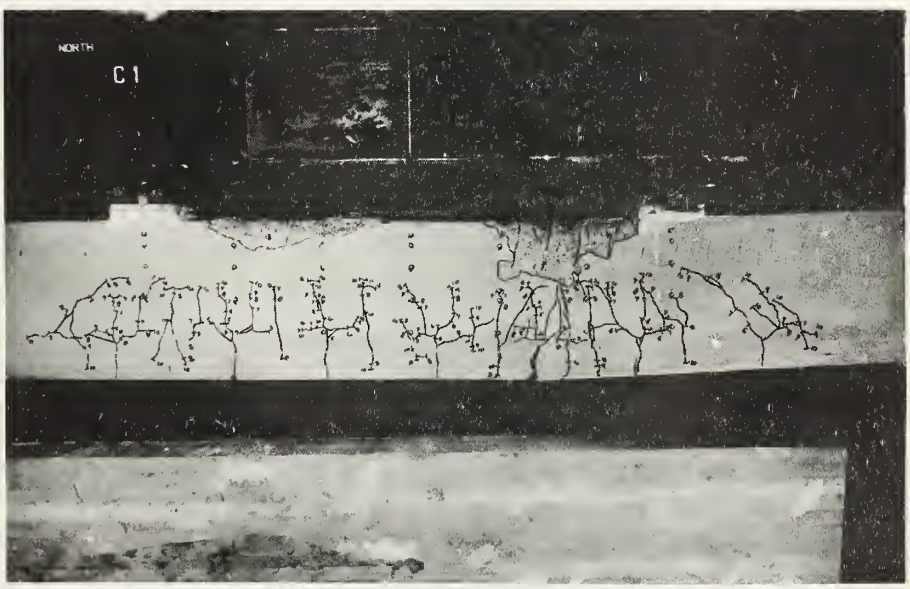


FIGURE 4.14 CRACK PATTERN OF A BEAM
FAILING IN COMPRESSION

flexural crack extension.

The effect of the presence of spiral reinforcement in the compression zone should be negligible during the second stage of behavior.

4.5.4 Third Stage of Behavior

The third stage of behavior was initiated at spalling. A typical load-deflection curve, shown in FIGURE 4.12 by CURVE A, indicates an immediate reduction of stiffness at first spalling. The beam, with reduced stiffness, deflected rapidly until equilibrium which formerly existed between the rectangular compressed concrete and the tension steel was regained. The upper limit of the third stage occurred when the strains in the steel became inelastic.

The behavior of the beams during the third stage depended on: the type and amount of confinement, concrete strength and amount of tension reinforcement. It can be seen from FIGURES 4.1 to 4.4 that the type of confinement used influenced the amount of reduction in beam stiffness at spalling and consequently the amount of deflection that occurred during the regain of equilibrium. The stiffness of the beams of Series A, which had a single large spiral, was significantly reduced at spalling; this can be observed from the curves in FIGURES 4.1 to 4.4. For beams of Series B the reduction in stiffness was not as apparent because of less spalling. It can also be seen that for beams, with a greater amount of concrete spalling from the compression zone, larger deflections were required to establish equilibrium. In general, the rate at which spalling occurred was directly proportional to the amount of spalling.

The spiral pitch was one measure of the amount of confinement used for each beam. Beams of Series C, which failed as a result of disruption of the confined compressed concrete, were incapable of developing a complete third stage of behavior because the reduced confinement did not adequately restrain the lateral dilation of the concrete. The compressive resistance of the confined concrete was not large enough to resist the moment required to develop inelastic tension steel strains.

The reduction in beam stiffness at spalling was greater for beams with high strength concrete. For beams with adequate confinement the concrete strength appeared to have little influence on beam behavior after spalling. For beams in which less confinement was used, concrete strength was an important factor. The increase in load capacity after spalling, for beams of Series C, was dependent on the amount of confinement and on the magnitude of the compression force which existed after stress redistribution. The magnitude of this force depended on the magnitude of the spalling moment and, therefore, the concrete strength.

The amount of tension reinforcement had a great influence on the extent of the third stage. All of the beams of Series A and Series B, with the exception of Beam A2, were capable of resisting loads greater than the spalling load by either full or partial development of the third stage. The typical load-deflection relationship for these beams is shown in FIGURE 4.12, CURVE A. Beam A2, which had a single large spiral and 6 tension strands failed in tension immediately after spalling. The third stage was very short in this case because the smaller amount of tension reinforcement was not able to sustain the great increase in

stress that occurred as a result of stress redistributions. Failure occurred by fracture of the strands at a load smaller than the spalling load. The typical load-deflection relationship for this type of behavior is shown in FIGURE 4.12, CURVE B.

Beam cracking during the third stage was affected by the presence of the spirals. The vertical flexure cracks, that had begun to "fork" out towards the end of the second stage, began to propagate in a horizontal direction at both the level of the bottom of the spirals and of the tension steel. Existing inclined cracks in the shear span extended during the third stage and additional inclined cracks formed.

### 4.5.5 Fourth Stage of Behavior

The fourth stage of behavior commenced when the tension reinforcement became inelastic. This stage was marked by a rapid increase in beam deflection for a small increase in load. The extent to which the fourth stage developed depended on the degree of confinement of the concrete and the percentage of tension reinforcement. For beams which had well confined concrete and the smaller amount of tension reinforcement the load-deflection curves showed well developed fourth stages of behavior. Beams A3, B2 and B3 displayed this behavior at loads significantly higher than the spalling loads. Beam A2 had a well developed fourth stage at a load which was smaller than the spalling load. Beams of Series C collapsed as a result of disruption of the concrete under reduced confinement, before inelastic strains developed in the eight tension strands. Those beams of Series A and Series B which failed by unbonding of the tension reinforce-

ment did not develop a fourth stage of behavior because the strands unbonded before inelastic strains could be developed.

## 4.6 Modes of Failure

### 4.6.1 General Remarks

The ultimate strength of the test beams depended on the strength of the confined concrete in the compression zone and on the tensile strength of the tension reinforcement. Three modes of failure were observed during the tests. All of the failures were classified as either tension, compression or bond failures. Each classification of failure was based on the factor initiating the final collapse of the members.

### 4.6.2 Tension Failure

Tension failures occurred when yield strains in the tension reinforcement developed before failure of the concrete in the confined core took place. Tension failures occurred suddenly as a result of fracture of the tension strands. The extremely ductile nature of this type of failure was due to two main factors: the ductile behavior exhibited by the interaction of the spirals and the confined inelastic concrete and ductile yielding of the tension steel. The tension steel of Beam C2 fractured even though the failure was initiated by disintegration of the confined concrete. This type of failure was classified as a compression failure and is discussed in the following section. A typical tension failure is shown in FIGURE 4.15.

### 4.6.3 Compression Failure

Compression failures occurred as a result of either failure of

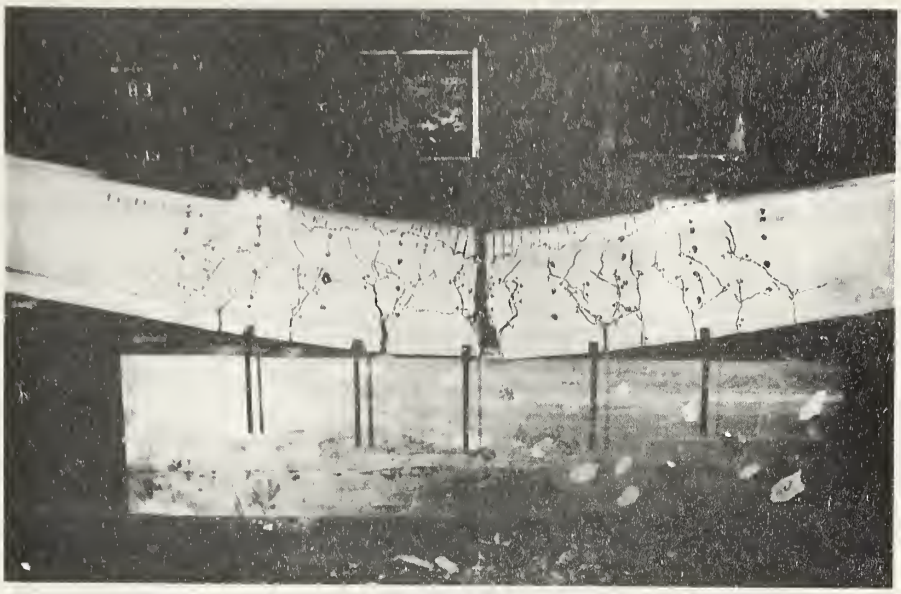


FIGURE 4.15 TENSION FAILURE [BEAM B3]

FIGURE 4.16 YIELDED SPIRAL [BEAM C3]

the spiral or failure in the concrete. Yielding of the spiral caused compression failures to occur in Beams C2 and C4. As a result of this yielding the magnitude of the confinement supplied by the spiral became constant even though concrete stresses and transverse strains continually increased. This, in effect, meant a reduction in confinement of the compressed concrete and the concrete within the spiral crushed rapidly. A spiral which has yielded is shown in FIGURE 4.16. The inability of the 3-in. pitch spirals of Beams C1 and C3 to confine the concrete resulted in crushing of the concrete between the spiral loops prior to any yielding of the spirals. Lateral displacements of the concrete in these areas were not restrained and disintegration of the compressed concrete occurred. Beams which failed in compression in the two ways discussed above are shown in FIGURES 4.17 and 4.18

The final collapse of beam C2 occurred as a result of fracture of the tension strands, even though disintegration of the compressed concrete was extensive. The initial disintegration of the compressed core caused the neutral axis to move down in the beam, therefore reducing the moment arm of the tension steel. To resist the applied moment the tension force in the strands was forced to increase and fracture occurred.

The degree of propagation of spalling throughout the constant moment region was considerably less for beams with the larger spiral pitches. Beam C3 which had a 3-in. pitch spiral, showed extensive spalling at only one location other than the location of the crushing failure. The remainder of the constant moment region showed little sign of spalling distress.

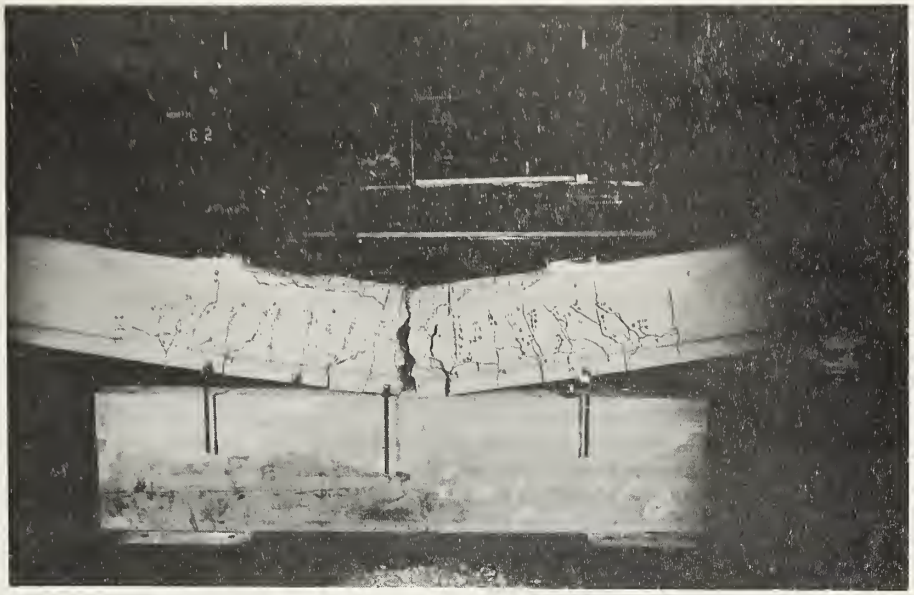


FIGURE 4.17 COMPRESSION FAILURE
[SPIRAL YIELD-BEAM C2]

FIGURE 4.18 COMPRESSION FAILURE
[ARCHING FAILURE-BEAM C3]

Compressive failures were not sudden like tension failures but occurred in a slow and ductile manner.

4.6.4 Bond Failure

Beams A1, A4, B1 and B4 failed by unbonding of the tension strands at load considerably higher than the spalling loads, but lower than the loads which would have been required to cause inelastic steel strains or failure of the confined compressed concrete. This loss of bond resulted in large deflections for small increases in load.

A typical bond failure is shown in FIGURE 4.19. It can be seen that the unbonding resulted in the formation of a series of diagonal cracks in the shear span. These cracks increased in width as unbonding progressed from the region of the load point towards the support. The neutral axis continued to move up in the beam because the confinement of the concrete prevented crushing. Even though the strands were completely unbonded from the load point to the end of the beam, the beam continued to resist small increases in load. The ultimate load was reached when the increase of the internal moment arm for an increase in load became very small. The unbonded strands could not resist the additional force applied at this stage and the beam deflected rapidly.

Beams A1 and B1 were tested with an 11-ft. span and a prestress transfer length of 8-in. at either end. Because unbonding occurred in these beams, the span length was reduced to 10-ft. and the prestress transfer length increased to 14-in. for tests of Beams A4 and B4. Despite the increased transfer length Beams A4 and B4 also failed by unbonding of the tension strands.

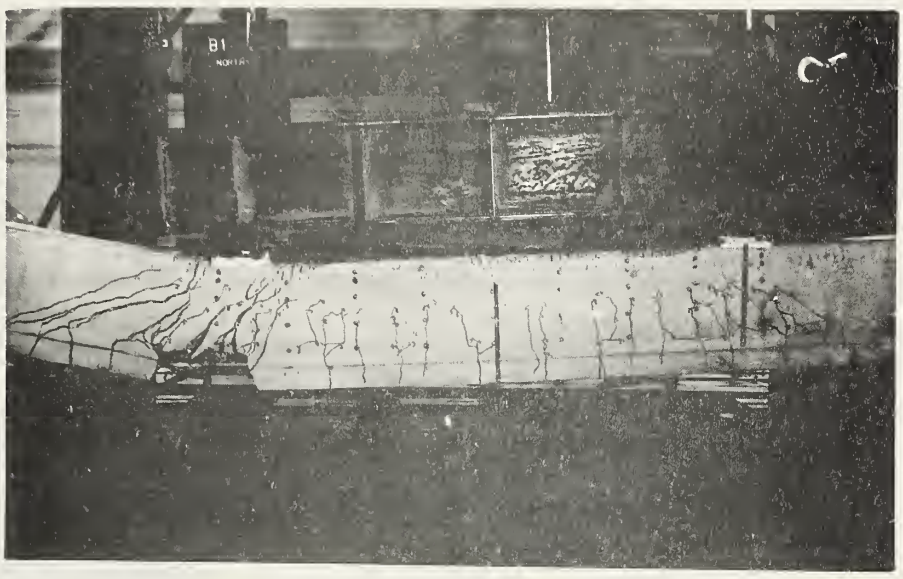


FIGURE 4.19 FAILURE THROUGH UNBONDING
[BEAM B1]

# CHAPTER V

# ANALYSIS OF TEST RESULTS

## 5.1 Introduction

This chapter is a brief outline of the methods used to determine the measured moment-curvature relationships on the basis of the strain and deflection data obtained during the beam tests. The derivation of a theoretical moment-curvature relationship prior to spalling is also discussed and comments are presented on the possibility of a strength analysis of the bound concrete section.

## 5.2 Computation of Moment-Curvature Relationships

### 5.2.1 General Remarks

A prestressed beam acts as a homogeneous elastic member only for stages of loading prior to cracking. Beyond the cracking load the characteristics of the cross-section vary from point to point. Because the curvature for any portion of the beam is dependent on the crack pattern, the relationship between moment and curvature varies along the length of the beam. No one section of the beam can be assumed to be representative of the behavior of the whole beam. The approximation of beam behavior must, therefore, be based on the relationship between moment and average curvature.

For beams which are loaded at two points symmetrical about midspan, the central region of the beam is subjected to constant moment. Curva-

ture can also be assumed constant throughout this region. The moment-curvature relationship can then be derived on the basis of the applied loads and average curvature.

### 5.2.2 Computation of Curvatures from Side Strains

Curvatures prior to spalling, and in some cases beyond spalling, were determined from the distribution of strains over the depth of the beam. Strains were averaged along the individual gage lines to determine an average strain distribution over the depth of the beam. Since the average strain distribution was linear, it was possible to determine the average curvature throughout the constant moment region by dividing the average strain on any one gage line by the distance from the gage line to the neutral axis.

### 5.2.3 Approximation of Curvatures from Deflections

At later stages of loading the compressive and tensile deformations across the gage columns became too large to be measured with the 8-in. Demec gage. Curvatures at subsequent increased loads were derived on the basis of the relative deflections which occurred between the five locations at which deflections were measured with the precise level. The derivation of the expression used to relate the average curvature to the relative deflections is presented in APPENDIX B. This method, because it is based on the assumption that horizontal distances between points on the beam remain constant, is at best only approximate.

The moment-curvature relationships for all beams are shown in FIGURES 5.1 to 5.3.

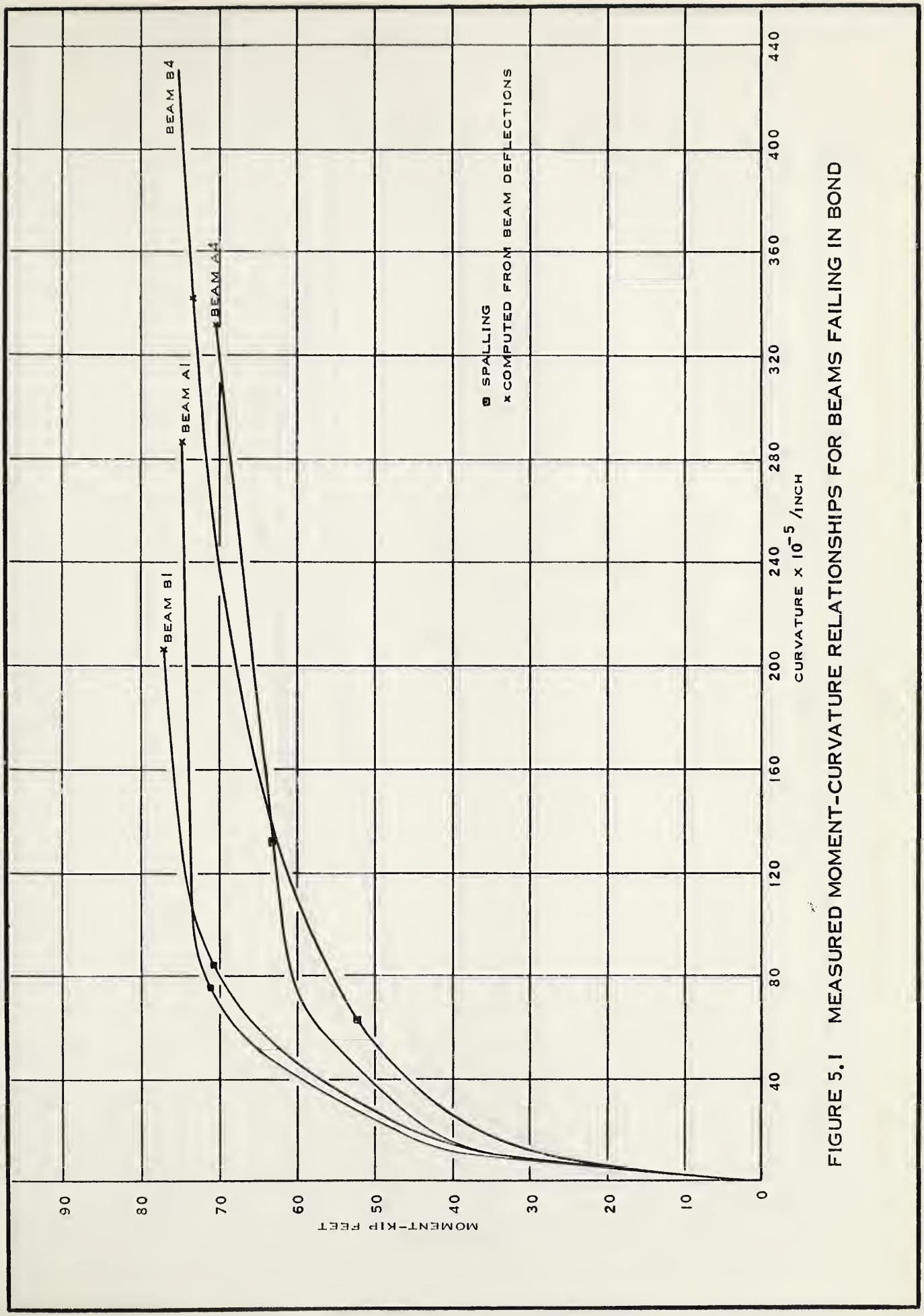


FIGURE 5.1 MEASURED MOMENT-CURVATURE RELATIONSHIPS FOR BEAMS FAILING IN BOND

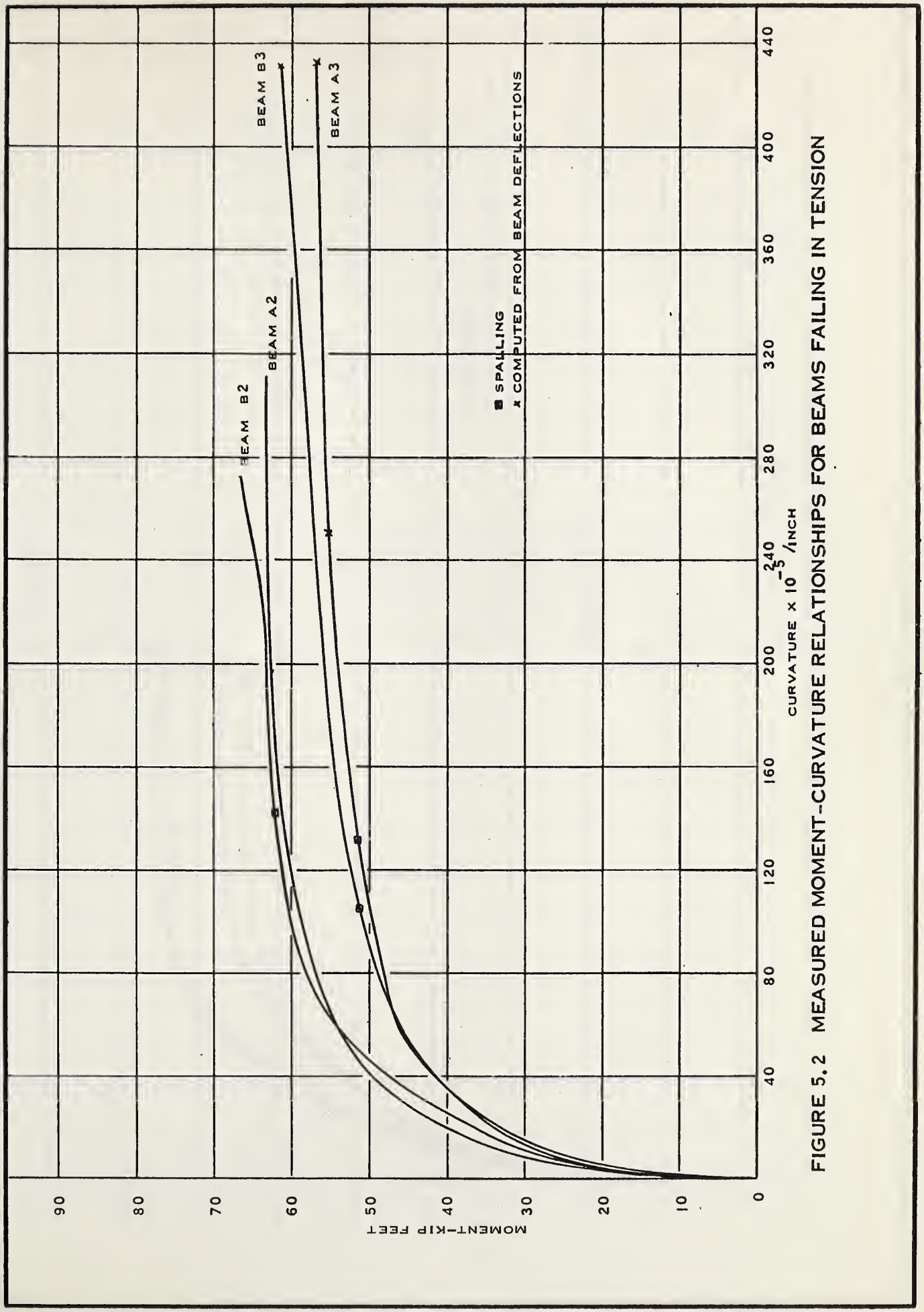


FIGURE 5.2 MEASURED MOMENT-CURVATURE RELATIONSHIPS FOR BEAMS FAILING IN TENSION

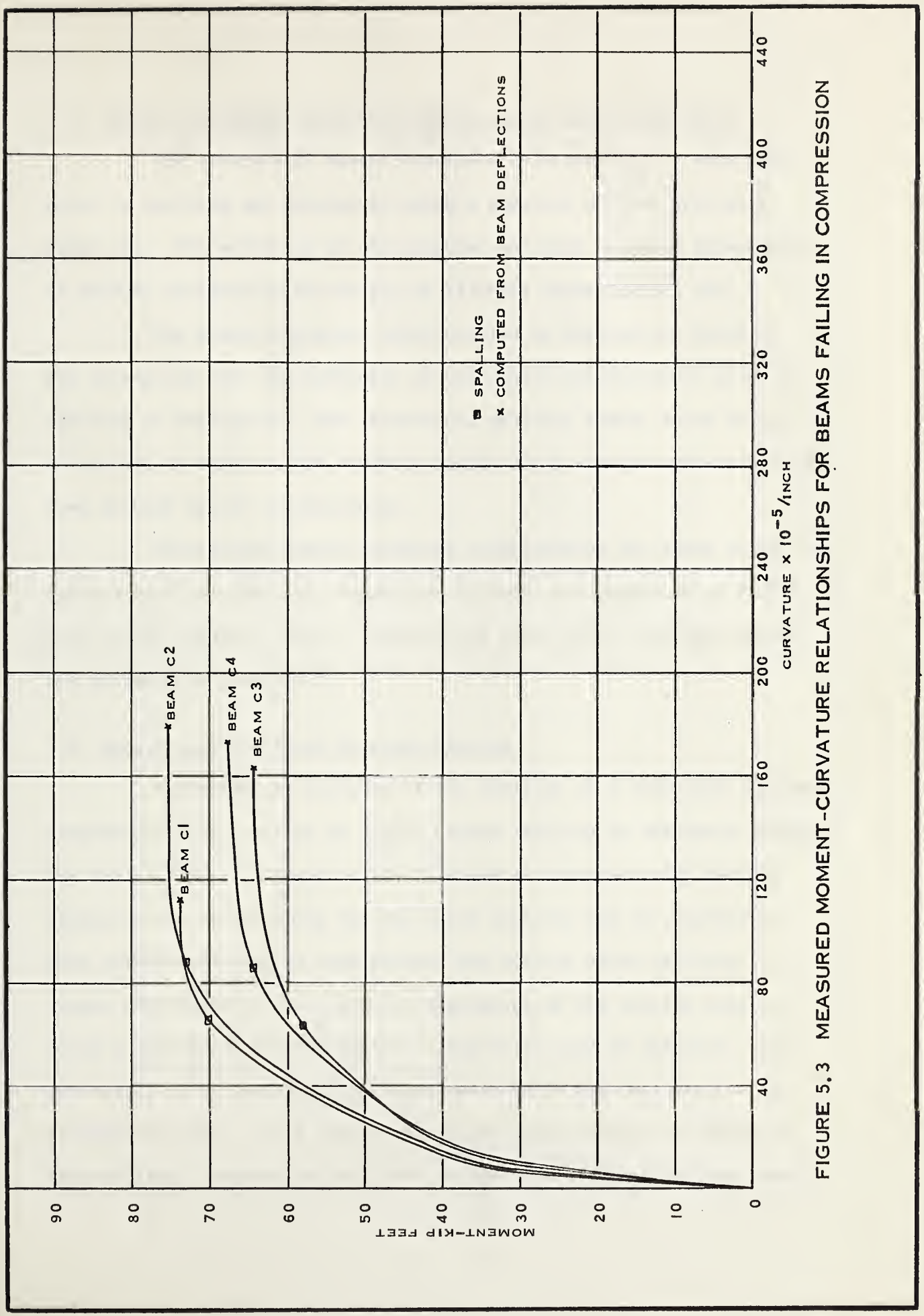


FIGURE 5.3 MEASURED MOMENT-CURVATURE RELATIONSHIPS FOR BEAMS FAILING IN COMPRESSION

## 5.3 Theoretical Moment-Curvature Relationship Prior to Spalling

The theoretical moment-curvature relationship for each beam prior to spalling was determined using a computer program written by Bakar (7). The mechanics of the computer analysis is based essentially on methods outlined by University of Illinois investigators (8).

The moment-curvature relationships so derived are based on the assumption that the influence of the spiral reinforcement prior to spalling is negligible. The theoretical spalling moment based on this assumption is equal to the crushing moment for a similar over-reinforced beam without spiral reinforcement.

Theoretical moment-curvature relationships for beams displaying typical bond, tension and compression failures are presented in FIGURE 5.4. Theoretical spalling moments and observed spalling and ultimate moments are presented in TABLE 5.1.

## 5.4 Analysis of the Bound Concrete Section

A theoretical analysis of the behavior of a beam with confined compression zone concrete at stages beyond spalling is extremely complex. The analysis must be based on some assumed or experimentally derived stress-strain relationship for the bound concrete and is complicated when circular binding is used because the section after spalling is no longer rectangular. This non-rectangularity of the section does not allow a simplified representative-stress-block type of analysis. The determination of the resultant compression force and its location is therefore complex. With a knowledge of the magnitude and location of the resultant compression force the analysis of a laterally bound beam

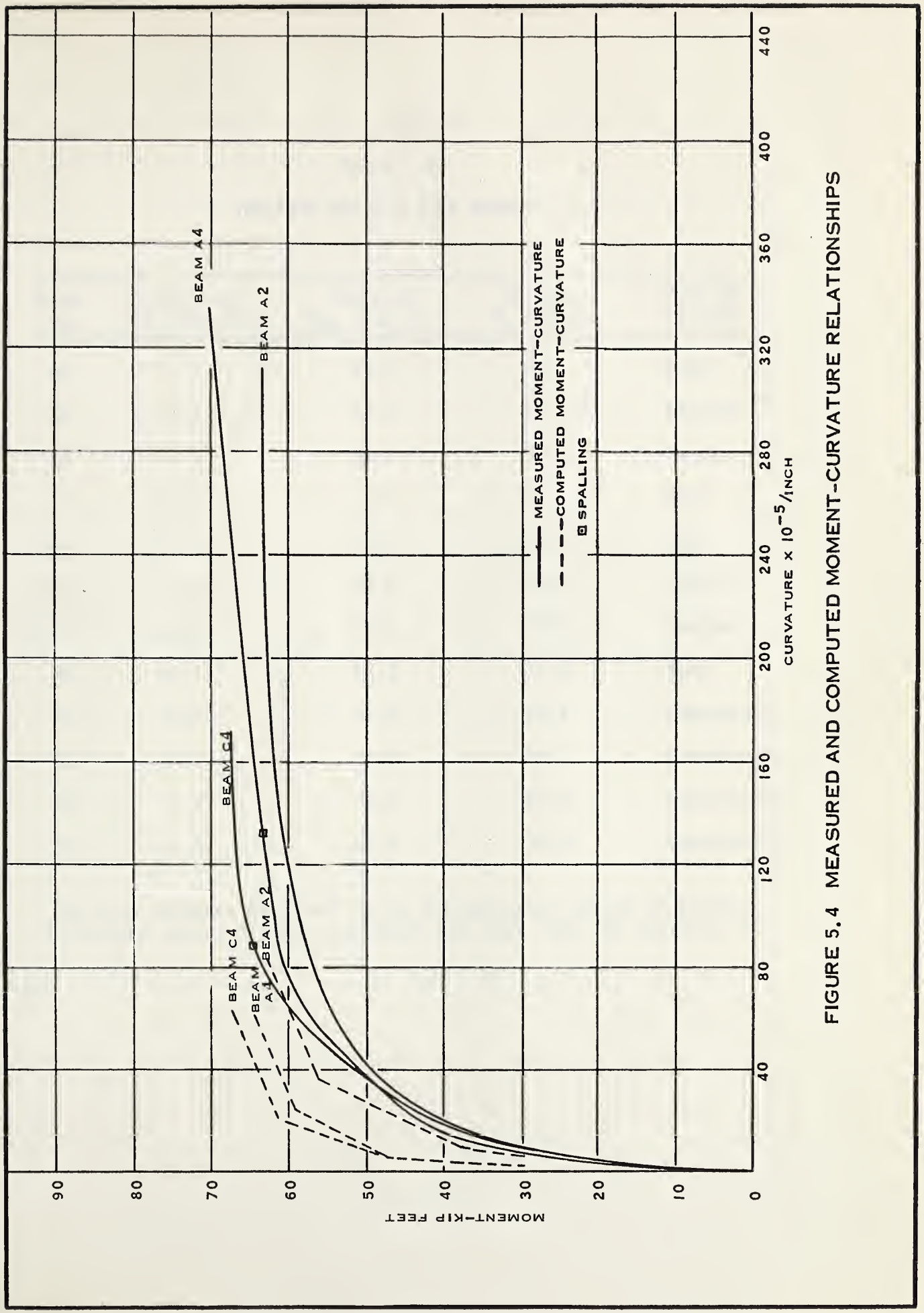


FIGURE 5.4 MEASURED AND COMPUTED MOMENT-CURVATURE RELATIONSHIPS

TABLE 5.1

SPALLING AND ULTIMATE MOMENTS

| Beam No. | Theoretical $M_{sp}$ (kip-ft.) | Observed $M_{sp}$ (kip-ft.) | Observed $M_u$ (kip-ft.) | Mode of Failure |
|---|---|---|---|---|
| A1 | 75.7 | 71.7 | --* | Bond |
| A2 | 62.9 | 65.1 | 63.3** | Tension |
| A3 | 54.2 | 51.3 | 59.4 | Tension |
| A4 | 64.5 | 63.3 | 70.2 | Bond |
| B1 | 77.2 | 70.2 | 79.8 | Bond |
| B2 | 61.9 | 63.6 | 69.4 | Tension |
| B3 | 52.8 | 51.3 | 63.9 | Tension |
| B4 | 62.5 | 52.2 | 77.8 | Bond |
| C1 | 75.9 | 70.2 | 75.7 | Compression |
| C2 | 75.9 | 73.2 | 76.2 | Compression |
| C3 | 67.5 | 58.2 | 67.2 | Compression |
| C4 | 67.5 | 64.2 | 72.3 | Compression |

*No true ultimate obtained due to discontinuous nature of loading
** Failure occurred under sustained load less than the spalling load

is possible using the methods and assumptions used in the analysis of ordinary prestressed beams.

Although a detailed analysis, as such, is beyond the scope of this investigation, recommendations shall be presented in subsequent sections to outline the possible range of testing further required to gain the information necessary for an analysis.

# CHAPTER VI

# DISCUSSION OF TEST RESULTS

## 6.1 Measured Load-Deflection Relationships

The measured load-deflection relationships are shown in FIGURES 4.1 to 4.6 and the four stages of behavior exhibited by these relationships are discussed in Section 4.5.

The load-deflection curve for Beam A1, at later stages of loading, is shown in FIGURE 4.1 as a broken line because the loading was discontinuous. The load was completely released at two load levels during this particular test to allow the placing of additional plates under the jack heads. Loading of all other beams was made continuous by the use of the pipe column described in Section 3.3.3. Beam B4, which had an initial warp in the lateral direction, and concave to the front face, deflected a considerable amount in the lateral direction during loading to failure. Consequently, the results of this test were poor and no valid comparisons can be made between the behavior of Beam B4 and the other beams.

The shape of the load-deflection curves, after cracking and prior to spalling, indicates the effects of the amount of tension reinforcement and the concrete strength, and is not significantly influenced by the spiral reinforcement in the compression zone. The effects of the amount of tension reinforcement are shown by comparison of FIGURES 4.1

and 4.2 and FIGURES 4.3 and 4.4. The effect of increasing the amount of tension reinforcement by a factor of 1.33 can be observed to be an increase in the load required to produce a given deflection by a factor of from 1.05 to 1.13. From a comparison of FIGURES 4.1 to 4.4 inclusively, the influence of variations in concrete strength can be observed. Comparisons of FIGURES 4.2 and 4.3 with FIGURE 4.1 and 4.4 and FIGURES 4.5 and 4.6 show that changes in concrete strength were more effective in changing the stiffness of beams with large amounts of tension reinforcement than for beams with lesser amounts of reinforcement.

The shape of the load-deflection curves after spalling is dependent on the type and amount of confinement, concrete strength and amount of tension reinforcement. For beams in which the lateral binding ratio was high, concrete strength had only a small influence on the shape of the load-deflection curves. As discussed in Section 4.5, the amount of tension reinforcement was sufficiently large that in no case did yielding occur prior to spalling.

The influence of the type of spiral used on the behavior of the beams can be observed by comparison of the load-deflection curves for beams of Series A with those for beams of Series B. The beams of Series A had one large spiral in the compression zone and the beams of Series B had two smaller spirals side-by-side. The reduction in stiffness, due to spalling, was significantly larger for the beams of Series A, because the amount of concrete spalling off was greater. This behavior was discussed previously in Section 4.5.4. Since the beams of Series B had less than half the amount of spalling that occurred in the beams of

Series A, the reduction in stiffness was much smaller. At stages of loading beyond spalling it can be seen that the load-deflection curves for Series B beams are above and essentially parallel to the curves for similar beams of Series A. The deflection required to regain equilibrium after spalling can be observed to be much smaller for beams in which the lesser amount of spalling occurs.

The influence of the amount of confinement is shown in FIGURES 4.5 and 4.6. The curves of FIGURE 4.5, which are for beams with high strength concrete, are nearly identical for loading up to failure. These curves indicate that there was a balance between conditions of compression failure by spiral yield for Beam C2 and the conditions of compression failure by arch breakdown for Beam C1. The ultimate deflection of Beam C2 was only about 15% larger than the ultimate deflection of Beam C1. Beams C3 and C4 which had the same binding ratios as Beams C1 and C2 respectively, .0116 and .0174, but had low strength concrete, had distinctly different load-deflection curves. The low strength concrete of Beam C3 was unable to arch between the 3-in. pitch spiral loops with the same degree of restraint as was supplied by the 2-in. pitch spiral of Beam C4. The load required to produce a given deflection was therefore higher for Beam C4 and failure occurred as a result of yielding of the spiral. The increase in ultimate deflection for the low strength concrete beams, obtained by increasing the lateral binding ratio by a factor of 1.5, can be observed from FIGURE 4.6 to be about 50%.

The effect of variation in concrete strength may be observed from comparison of FIGURES 4.1 and 4.3 with FIGURES 4.2 and 4.4 respectively.

It can be seen that the deflection required to regain equilibrium after spalling was larger for the beams with higher concrete strength. When the lateral binding ratio was high, concrete strength had little influence on beam behavior after equilibrium had been reached. As previously observed from comparison of FIGURES 4.5 and 4.6, concrete strength became a definite factor in the shape of the load-deflection curves when the lateral binding ratio was low enough that compression failures occurred.

The influence of the amount of tension reinforcement may be observed from comparison of FIGURES 4.1 and 4.3 with FIGURES 4.2 and 4.4, respectively. Beam A2, which had a low value of $P/f'_c$ factor failed by fracture of the tension reinforcement immediately after spalling, while Beam A1, which had the same concrete strength and spiral reinforcement but a larger amount of tension reinforcement, was able to resist the increased steel force imposed by spalling without development of yield strains. In all beams which were tension reinforced with 8 strands unbonding occurred before yield stresses in the steel or crushing of the confined concrete could take place. It was possible, for beams with 6 tension strands, to obtain ductile tension failures with large midspan deflections, through the use of adequate binding in the compression zone. All beams, except Beam A2, which had a low $P/f'_c$ value and single large spiral, were capable of maintaining elastic tension steel behavior throughout the large deflections associated with the establishment of equilibrium after spalling. The fourth stage of behavior was exhibited only by beams A2, B2, A3 and B3 which failed as a result of tension steel fracture, and was initiated in these beams at loads considerably higher than the

spalling loads.

Ultimate deflections for beams failing in tension were observed to be as high as 7 inches. The magnitude of ultimate deflection of these beams was generally about five times the spalling deflection and about thirty to forty times the cracking deflection. Beams failing in bond did so at midspan deflection in the order of 6-in. The result of reducing the amount of confinement of the compression zone was a reduction of the ultimate deflection to about 4-inches and failure of the beam by compression zone crushing.

## 6.2 Measured Moment-Curvature Relationships

The methods of computing the moment-curvature relationships are outlined in Sections 5.2 and 5.3 and the derived relationships are shown in FIGURES 5.1 to 5.3. These relationships, like the load-deflection relationships, display four stages of behavior. The extent of the individual stages and the shape of the resulting moment-curvature curves is dependent on the material properties and on the nature of the lateral binding in the compression zone.

No curvatures at failure could be directly computed since only the midspan deflection was measured at later stages of a beam test. The measured moment-curvature relationships presented in FIGURES 5.1 to 5.3 do not, therefore, show the ultimate curvatures. For purposes of comparison, the curvatures at failure for some beams are estimated in Section 6.5, on the basis of the magnitude of the ultimate midspan deflections.

The first stage of behavior represents the condition of elastic concrete and steel and corresponds to the initial linear portion of the

moment-curvature relationship. The upper limit of this stage was marked by the formation of flexural cracks. Upon initiation of the second stage, the rate of change of curvature with respect to moment increased as a result of the upward movement of the neutral axis. The third stage began at spalling and was characterized by a very rapid increase in curvature at a reduced beam stiffness. It was impossible to obtain a complete history of the moment-curvature relationship throughout this stage due to the sudden nature of the increase in curvature that occurred at spalling. The measured moment-curvature relationships do not, therefore, indicate the points of discontinuity that actually occurred at spalling. The fourth stage of behavior was initiated when the tension steel became inelastic. Large increases in curvature occurred for small increases in load throughout this final stage.

The shape of the moment-curvature curves prior to spalling was greatly influenced by the properties of the materials that made up the beam cross-sections and also appeared to be dependent to some degree on the confinement of the compressed concrete. Although the span length was slightly larger for Beams A1 and A2 than for the other beams tested and small variations in prestress did occur, the influence of small changes in these parameters shall not be considered in the following discussions.

The influence of changes in the amount of tension reinforcement, for constant concrete strength, can be observed from comparison of FIGURES 5.1 and 5.2. An increase of the amount of tension reinforcement by a factor of 1.33 caused an increase in the moment required to produce a

given curvature by a factor of from 1.20 to 1.30 for beams with high strength concrete and from 1.10 to 1.20 for beams with low strength concrete.

The influence of concrete strength prior to spalling may be observed from comparisons of FIGURES 5.1 and 5.2. The result of increasing concrete strength was an increase in the moment required to produce a given curvature.

Comparisons between curves in FIGURES 5.1 to 5.3 can be made to show the influence of the type and amount of lateral confinement on beam behavior. Definite trends in the moment-curvature relationships shown in FIGURES 5.1 and 5.2 indicate that the presence of the confining reinforcement did influence the shape of the curves prior to spalling. The moment curvature relationships for the beams of Series A, because they plot in all cases to the left of the curves for similar beams of Series B, indicate that the influence of type of spiral, even prior to spalling, was significant. The single large spiral of Series A beams caused a greater increase in the compression resistance of the confined elastic concrete because the area of concrete confined was larger than that for the smaller spirals. The neutral axis, at any given curvature, was lower in beams with the smaller spirals and the steel strains were therefore less. Even though the resultant compressive force was located higher in the beam and the internal moment arm of the steel was greater, the resisting moment was smaller at any given curvature. Comparison of the moment-curvature relationships for beams of Series C with similar beams of Series A and Series B show that variation in spiral pitch had

little influence on beam behavior prior to spalling. The curve for Beam C1 which had a 3-in. pitch spiral is not significantly different from the curve for Beam A1 which had a spiral 1-in. pitch.

The influence of increasing the amount of tension reinforcement by a factor of 1.33 was an increase in the moment required to cause a given curvature by a factor of from 1.15 to 1.20 for all beams of Series A and Series B after spalling. This shows that, for beams with a high lateral binding ratio, the influence of changes in amount of tension reinforcement is independent of the concrete strength after spalling has occurred.

From the curves of FIGURES 5.1 and 5.2 it can be seen that changes in concrete strength resulted in changes of the shape of the moment-curvature relationships after spalling. The curves for beams with high strength concrete levelled off after spalling, while the curves for the low strength concrete beams continued to rise gradually. This indicates that the neutral axis was lower in the low strength beams for any given curvature. The tension reinforcement of the high strength beams therefore became inelastic or unbonding occurred at lower curvatures and upward movement of the neutral axis was small. The neutral axis in the low strength beams continued to move upwards increasing the internal moment arm of the tension steel. The resisting moment of these beams continued to increase with increasing curvature until tension steel yielding or unbonding occurred.

The effect of the type of spiral used may be observed from comparison of the curves for Series A beams with those of Series B beams. From FIGURES 5.1 and 5.2 it can be seen that the moment required to produce

a given curvature after spalling was greater for beams with two smaller spirals than for beams with the single large spiral. The influence of the amount of confinement can be observed from comparison of FIGURES 5.1 and 5.3. Beams A1, A4, B1 and B4 all had spiral of 1-in. pitch and failed by unbonding of the tension strands. The result of increasing the spiral pitch to 2 and 3-in. for beams of Series C was a change in the mode of failure and also a considerable reduction of the ultimate curvature. The reduction in ultimate moment, caused by an increase in spiral pitch, was greater for beams with low strength concrete because the lower strength concrete was not able to bridge across between the adjacent spiral loops as well as higher strength concrete.

The confinement derived from the presence of rectangular stirrups has been shown to be small compared to the confinement supplied by spiral reinforcement (1) (3). The effects of the presence and variations in amount of shear reinforcement was, therefore, assumed negligible in the preceding discussions.

## 6.3 Comparison of Measured and Theoretical Moment-Curvature Relationships Prior to Spalling

Measured and theoretical moment-curvature relationships for typical beams failing in compression, tension and bond are shown in FIGURE 5.4. Although the measured and theoretical spalling moments, shown in TABLE 5.1, compare reasonably well, the observed curvatures at spalling are larger that the theoretical values. The discrepancy between the theoretical relationship, which assumes no spiral influence prior to spalling, and the measured relationship is typical of the re-

sults obtained for all the beams. Indications are that the influence of the spiral reinforcement, prior to spalling and especially after initial flexural cracking, is not negligible. Three reasons for this behavior can be suggested:

(1) The lateral confinement supplied by the spirals, even during elastic concrete behavior prior to spalling, restrained the neutral axis at a lower level than normally would be expected in an ordinary beam.

(2) The compressed concrete area was reduced by the presence of the spiral reinforcement.

(3) During casting of the concrete within the spirals the degree of uniformity and compaction of this concrete may not have been as high as that for similar beams with unconfined compressed concrete.

Previous investigators (1), (3) have stated that the presence of confinement has little or no influence on beam behavior prior to spalling. The majority of the theoretical and observed load-deflection curves given by Chan (3) do indicate definite influence of the confining reinforcement prior to spalling. If, in fact, the increase in curvature caused by the presence of the binder is due to a lower position of the neutral axis, the discrepancy would have been more noticeable if moment-rotation relationships had been derived. Base and Read (1) conducted tests on single point-loaded beams with only relatively small amounts of confinement. The disadvantage of single point-loaded tests is that a complex stress condition exists beneath the bearing plates which are at the point of maximum

moment. The influence of the confinement prior to spalling could not be readily observed. Also, any effects of confinement would not have been large for these tests because the amount of confinement was, for all beams, relatively small. In most of the beams, the area of confined concrete was significantly smaller than the total compressed area due to a 1/4-in. spiral cover and a 3/4-in. stirrup cover. The influence of the confining reinforcement prior to spalling would be less noticeable under these conditions.

## 6.4 Measured Spiral Strains

Measured spiral strains are shown in FIGURES 4.8 to 4.11 and the experimentally derived load-strain curve for the spiral steel is shown in FIGURE 3.2. For the beams of Series A and Series B, which had spirals of 1-in. pitch, the measured strains are an indication of how near to yielding the spirals were at failure of the beams. The yield strain of the cold-worked reinforcement was found to be on the order of 0.0017 in/in. Magnitudes of strain as high as 0.0014 were recorded at the top of the spirals of beams failing by fracture of the tension reinforcement and 0.0015 for beams at initial bond failure, with values as high as .0017 recorded for continued loading after initial bond failure.

The strain versus midspan deflection curves in FIGURES 4.8 to 4.10 show a considerable "scatter" of points. At earlier stages of loading, spiral strains, particularly for beams of Series B which had overlapping spiral with 1-in. pitch, were compressive strains. The occurrence of compressive strains appears to have been a consequence of collapse of small initial voids between the concrete and the spiral reinforcement.

The strain gages for Beam C1 became unattached from the spiral early in the test and no values are presented.

Even though the strains recorded appear random in nature the following general trends can be observed;

(1) From comparison of FIGURES 4.8 and 4.9, it can be seen that the strains at the top of the spirals at failure were larger than the strains at the side of the spirals.

(2) For any given midspan deflection and spiral type the strains in the spirals were greater for low strength concrete.

(3) From comparison of spiral strains for Series A beams with those for similar Series B beams, it can be seen that strains in the larger spirals were greater at any given deflection.

(4) The average strain at the top of the spirals was .0004 in/in at spalling with values as high as 0.0007. This indicates that the spirals did supply considerable confinement prior to spalling.

(5) Comparison of FIGURE 4.10 with FIGURES 4.8 and 4.9 shows that the spiral strains at early stages of loading were dependent on the beam deformations. At later stages of loading the spiral strains became dependent on the spiral pitch as well.

(6) FIGURE 4.11, which shows a typical spiral strain versus beam load relationship, indicates the behavior for beams with overlapping spirals. Prior to spalling the strain in the spiral was greater at the side than at the top. After spalling and at failure the strains at the top of the spiral were larger than at the side.

(7) From FIGURE 4.10 it can be seen that spiral yield took place in Beams C2 and C4, which had spirals of 2-in. pitch. For similar beams, C1 and C3, which had 3-in. pitch spirals, arch failure of the concrete occurred when spiral strains were in the order of 0.0010 in/in.

## 6.5 Comparison of Behavior of Beams with Confined and Unconfined Concrete

Previous investigators at the University of Alberta (5) (6) have reported on tests of beams similar to those tested during this investigation but with unconfined concrete. Of the beams tested by Raffa (6) and Belke (5), it was found that two beams (one from each investigation) were very close to the same as some beams of this investigation. Both of the beams had a span length of 11'-0" and a constant moment region of 5'-0". The dimensions of the beams were the same as for the beams discussed in this paper except that the overall depth of the beam tested by Raffa (6) was 12-in. Other details of the beams are shown in TABLE 6.1 below.

TABLE 6.1

PREVIOUS UNCONFINED BEAM TESTS

| Investigator | Beam No. | Concrete Strength $f'_c$ (psi) | $A_s$ ($in^2$) | Effective Prestress (ksi) | Mode of Failure |
|---|---|---|---|---|---|
| Belke | 13 | 3390 | .3468 | 137 | Compression |
| Raffa | 6 | 5390 | .3468 | 123 | Compression |

It can be seen that Beam 13 was similar to Beams A3 and B3 reported on in this paper and Beam 6 was similar to Beams A2 and B2.

For comparison of behaviors the measured moment-curvature relationships for the two unconfined beams above and the four similar confined beams of this investigation are shown in FIGURE 6.1. The curves for the unconfined beams are typical for over-reinforced beams failing in compression. The failures which occured in these beams were explosive and brittle failures and exhibited very little ductility.

As discussed previously in Section 6.2, it was not possible to obtain measured curvature values at failure. For purposes of comparison it was necessary to estimate the ultimate curvature by assuming that the moment-curvature relationship at later stages of loading is a direct reflection of the shape of the load-midspan deflection relationship. The ultimate curvature could then be approximated by multiplying the last measured curvature by the ratio of the ultimate deflection to the deflection at which the largest measured curvature occurred. In this manner the curvatures at failure for Beams A2, B2, A3 and B3 were estimated to be in the order of 350, 410, 570 and 530 x $10^{-5/in.}$ respectively.

Since the concrete strength, effective prestress and, in the case of Beam 6 (Raffa), cross-sectional dimensions of the previously tested unconfined beams were not completely the same as for the similar beams of this investigation, only general comparison can be made between the behavior of the two types of beams. It can be seen from FIGURE 6.1 that, through the use of adequate confinement, it was possible to increase considerably the ultimate curvature of a normally over-reinforced beam.

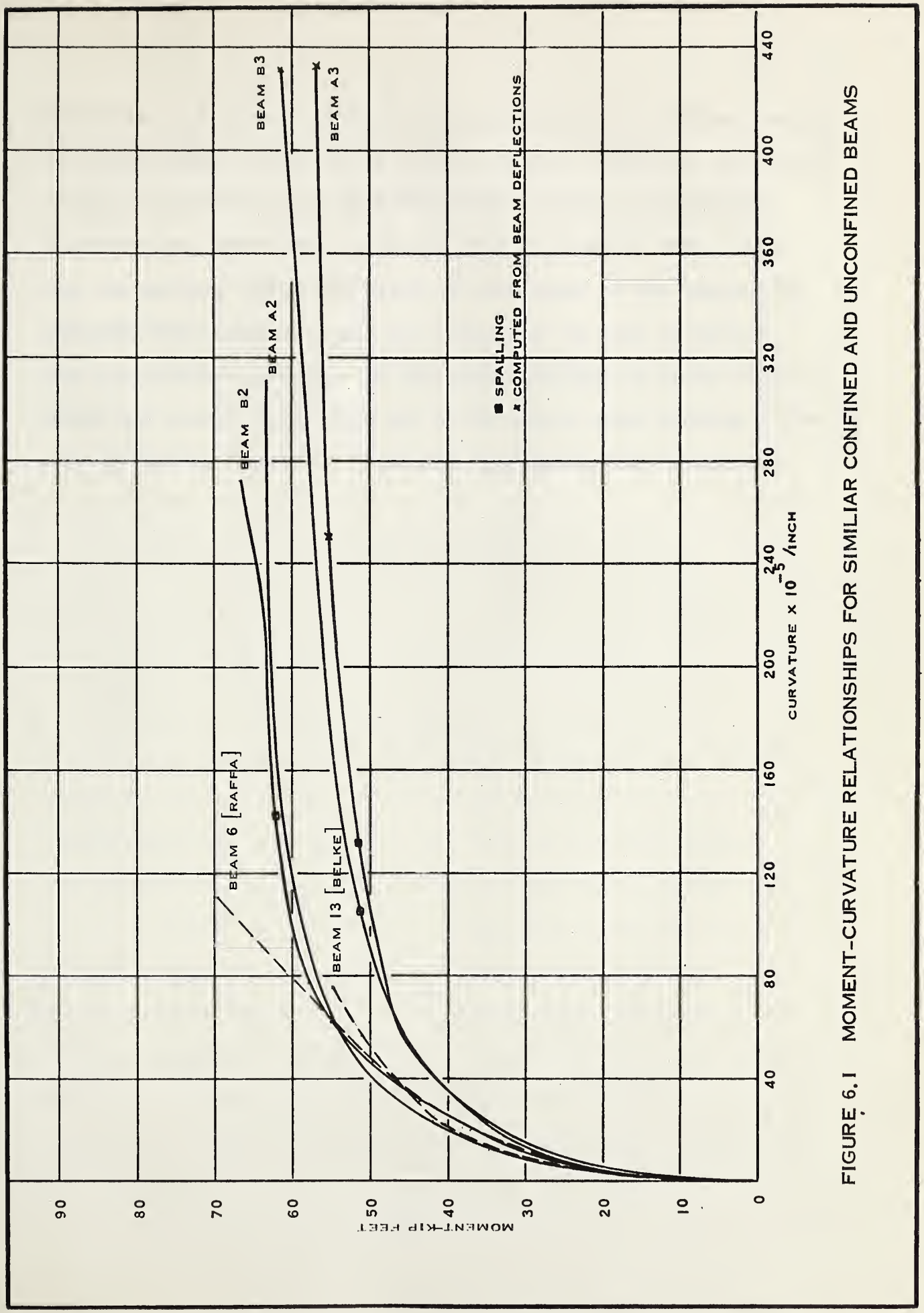


FIGURE 6.1 MOMENT-CURVATURE RELATIONSHIPS FOR SIMILIAR CONFINED AND UNCONFINED BEAMS

Indications are, from this figure, that the increase in curvature possible for high strength concrete beams can be as high as four-fold, and as high as five to six-fold for low strength concrete beams. For all beams, except Beam A2, these large curvatures were developed at loads higher than the spalling loads. The result of confinement of the concrete for moderately over-reinforced beams was a change of the mode of failure from compression to tension. In this manner the ductile nature of the spiral and concrete interaction and of the tension steel yielding process were utilized to develop a ductile beam load-deformation relationship.

# CHAPTER VII

# SUMMARY, CONCLUSIONS AND RECOMMENDATIONS

## 7.1 Summary

Three series of prestressed concrete beams, with lateral confinement in the compression zone, were tested. All of the beams were two-point loaded symmetrically about midspan and all but two beams were tested with a 10'-0" span length and a constant moment region of 4'-0". The first series consisted of four beams having a single large spiral of constant pitch in the compression zone. The variables for this series were amount of tension reinforcement and concrete strength. The second series was the same as the first series except that two smaller spirals placed side-by-side were used to confine the compressed concrete. The last series also consisted of four beams. The variables of this series were spiral pitch and concrete strength while the type of spiral and amount of tension reinforcement were held constant. The level of prestress, although it was intended to be constant for all twelve beams tested, varied slightly.

Measurements of strains over the depth of the beam and at the extreme compression fibre were taken. Strains were also measured at two locations in the spiral. The deflections of the beam were also measured at five locations. Load-deflection and moment-curvature relationships were determined from these measurements. Theoretical moment-curvature relationships prior to spalling were calculated using a computer program (7) and

comparisons were made between the theoretical and observed curves. Comparisons were also made between the observed behavior of the confined beams and the behavior of similar unconfined concrete beams tested by previous investigators at the University of Alberta (5) (6).

## 7.2 Conclusions

On the basis of the results obtained from the beam tests, and a study of the behavior of the beams, some conclusions have been formulated with regard to the behavior of bonded prestressed concrete beams having confined compressed concrete. These conclusions are presented in the following paragraphs under three classifications: general behavior, behavior prior to spalling and behavior after spalling.

The following conclusions are based on observations regarding the general behavior of bound concrete beams:

(1) The use of spiral confinement of the compressed concrete was found to be very effective in producing ductile failures in beams which under normal conditions were over-reinforced.

(2) The use of two smaller overlapping spirals was found to be superior to a single large spiral because the reduction in beam stiffness at spalling was smaller.

(3) The limiting compressive strain in the concrete at spalling was found to be on the order of .004 in/in. with values as high as .006 in/in.

(4) The amount of confinement derived from the rectangular shear reinforcement was considered to be small enough in comparison to spiral reinforcement that it could be neglected.

The following conclusions pertain to the observed beam behavior prior to spalling:

(5) Indications were that the presence of spiral confinement did influence the behavior of the beams prior to spalling. This conclusion is based on the following observations:

(a) For any beam, the observed curvature at any given moment was larger than the theoretical curvature which was calculated assuming no spiral influence prior to spalling.

(b) The curvature at any given moment, prior to spalling, was larger for the beams with two small spirals than for similar beams with a single large spiral in the compression zone.

(c) The average spiral strain at spalling was found to be on the order of .0004 in/in. This strain represented a spiral force of about 0.6 kips and indicated that the confinement supplied by the spiral prior to spalling was significant.

(6) For the over-reinforced beams tested, increasing the concrete strength increased the moment required to produce an increment of beam deformation prior to spalling.

(7) For a constant prestress, increasing the amount of tension reinforcement resulted in reduction of beam deformation at a given load prior to spalling.

The following conclusions are based on the observed beam behavior after spalling:

(8) The deflection required to establish equilibrium after spalling was larger for beams with the single large spiral than for beams with the two smaller spirals. Beams with high strength concrete also deflected a larger amount during establishment of equilibrium than did beams with low strength concrete.

(9) It was possible, through the use of adequate concrete confinement, to increase the compressive capacity of a over-reinforced beam to such an extent that the ordinarily brittle compression failure could be transformed to a more ductile tension failure or to a bond failure.

(10) Compression failures of beams with lesser amounts of confinement were observed to occur in two ways: yielding of the spiral and concrete arch failure.

(11) The ultimate moment and curvature of beams with large amounts of confinement were dependent mainly on the amount of tension reinforcement and only slightly on the concrete strength.

(12) The reduction of ultimate moment and curvature, associated with an increase in spiral pitch, was smaller for beams with high strength concrete than for similar beams with low strength concrete.

## 7.3 Recommendations

Investigators (1) (2) have shown that spiral confinement of the concrete is effective as a means of improving the moment-rotation characteristics of over-reinforced beams. A study of the rotational

capacity of confined axially-loaded specimens is also reported (3). To date, no attempt has been made to derive the expressions required to predict strength and load-deformation relationships for confined concrete beams.

The main difference between ordinary beam analysis and the analysis for bound beams* is the nature of the stress-strain relationship for the concrete. It is apparent that the object of future investigations should be the derivation of the bound concrete stress-strain relationship as pertaining to beams.

Two methods of derivation might be used. Firstly the stress-strain relationship might be obtained from tests of axially-loaded confined specimens at small eccentricities. The important variables of such a series of tests would be lateral binding ratio, concrete strength and eccentricity. The incorporation of the stress-strain relationship, determined in this manner, into the beam analysis would be based on a trial-and-error solution to satisfy both compatibility of concrete and steel strains and compressive and tensile forces. The second alternative would be to conduct a further series of beam tests such as that suggested below. The results of these tests and of the tests reported in this thesis could then be utilized to determine the co-ordinates of the bound concrete stress-strain relationship in terms of the parameters associated with the beam cross-sectional dimensions and material strengths. The important variables which should be considered in such a test series are:

---

*A suggested flexural strength analysis is presented in APPENDIX A.

(1) amount of tension reinforcement

(2) amount of confinement; spiral pitch

(3) concrete strength

The following recommendations are presented as a guide to future investigators in planning and conducting the next series of tests:

(1) All beams tested should be two-point loaded. The prestress transfer length should be increased for highly over-reinforced beams to eliminate bond failures.

(2) Confinement should be obtained from two small, overlapping spirals in the compression zone. The load-deformation characteristics of beams with this type of spiral confinement have been shown to be superior to those for beams with a single large spiral.

(3) Extensive beam instrumentation should be used to record completely the beam load-deformation relationships during and after spalling and to measure accurately beam curvatures up to failure. The following alternatives are possible in this respect:

(a) The automatic Amsler load-deflection plotter might be used to plot the complete load-deflection relationships.

(b) A number of precise levels might be used at later stages of loading to record simultaneously the deflection readings at many points along the beam.

(c) Micrometer inclinometers might be used at many points throughout the beam span to record rotations from which curvatures to failure could be derived.

(4) The measured curvatures and respectively neutral axis locations, as observed from the upper level of flexural cracking, at various increasing applied moments to failure could be used to obtain the bound concrete stress-strain relationship. With a knowledge of the extreme compression fibre strain and total compressive force at each load increment the derivation of the complete stress-strain relationship would be based on an iterative procedure. This analysis might best be carried out using a computer program.

Using the stress-strain relationship for the bound concrete as determined from the above tests, strength and load-deformation expressions, similar to those for normal beams, could be derived.

A further investigation, based on the results of the test series recommended above, might be a study of the behavior of two-span continuous beams which have bound concrete. In this manner, the feasibility of basing limit design procedures on the strength and load-deformation expressions, using the procedures recommended above, could be studied.

## LIST OF REFERENCES


1. Base, G.D., and Read, J.B., "Effectiveness of Helical Binding in the Compression Zone of Concrete Beams", Journal, American Concrete Institute, July 1965, p. 763.

2. Base, G.D., "Helical Reinforcement in the Compression Zone of Concrete Beams", Concrete and Constructional Engineering (London), Vol. 57, No. 12, December 1962, p. 456.

3. Chan, W.W.L., "The Ultimate Strength and Deformation of Plastic Hinges in Reinforced Concrete Frameworks", Magazine of Concrete Research. No. 21, November 1955.

4. Blume, J.A., Newmark, N.M. and Corning, L.H., "Design of Multistory Reinforced Concrete Buildings for Earthquake Motions", Portland Cement Association, 1961.

5. Belke, T., "Deformation Characteristics of Pretensioned Concrete Beams Subjected to Bending and Shear", M.Sc. Thesis, University of Alberta, May 1965.

6. Raffa, G., "Deformation Characteristics of Pretensioned Concrete Beams in Flexure", M.Sc. Thesis, University of Alberta, October, 1964.

7. Bakar, L.J., "Analysis of Strength and Deformations for Bonded Prestressed Concrete Beams", M.Sc. Thesis, University of Alberta, April, 1966.

8. Warwaruk, J., Sozen, M.A. and Siess, C.P., "Strength and Behavior in Flexure of Prestressed Concrete Beams", University of Illinois, Experimental Station Bulletin No. 464, August 1962.

9. Neville, A.M. "Properties of Concrete", Pitman and Sons, 1963.

10. Portland Cement Association, "Design of Concrete Mixtures", Structural Series Bulletin No. 100, 1963.

11. American Concrete Institute, "Building Code Requirements for Reinforced Concrete, (ACI 318-63)", June 1963.

# Appendix A

# NOTATION AND ANALYSIS

## A.1 Notations

### Cross-sectional Dimensions

$A$ = cross-sectional area of beam before spalling

$A_s$ = area of prestressed tension reinforcement

$A_s''$ = cross-sectional area of spiral reinforcement

$a$ = spiral pitch

$\bar{D}$ = diameter of confined concrete

$b$ = width of rectangular beam

$d$ = effective depth of beam

$I$ = gross moment of inertia of concrete cross-section about the centroidal axis

$e$ = distance from beam centroidal axis to the resultant prestressing force

### Forces and Moments

$C$ = total compressive force in the concrete

$T$ = total tensile force in the tension reinforcement

$P$ = total effective prestressing force

$M_u$ = resisting moment of the beam at failure

$M_{sp}$ = resisting moment of the beam at spalling

$M_{cr}$ = resisting moment of the beam at initial flexural cracking

### Stresses

$f_c'$ = compressive strength of concrete determined from tests on 6 x 12-in. control cylinders

$f_{cu}'$ = equivalent confined concrete stress

$f_c$ = equivalent concrete strength for bound axially-loaded specimens

$f_r$ = modulus of rupture of the concrete

$f_{se}$ = effective prestress

$f_{su}$ = stress in prestressed reinforcement at failure

$f''_s$ = stress in spiral reinforcement

$f_e$ = limiting elastic compressive stress for concrete

$f_p$ = limiting plastic compressive stress for concrete

$f_u$ = ultimate strength of confined compressed concrete

$c_u$ = unconfined cube compressive strength of concrete

Strains

$\epsilon_{ce}$ = strain at level of tension reinforcement due to effective prestress

$\epsilon'_{sa}$ = increase in strain in the prestressed reinforcement during loading to failure

$\epsilon_{se}$ = effective prestrain due to effective prestress

$\epsilon_{su}$ = strain in prestressed reinforcement at failure

$\epsilon_e$ = limiting elastic compressive strain for concrete

$\epsilon_p$ = limiting plastic compressive strain for concrete

$\epsilon_u$ = ultimate confined concrete compressive strain

Dimensionless Factors

$K''_u$ = ratio of depth of neutral axis at failure to effective depth

$K''_2$ = ratio of depth to resultant compressive force to depth of neutral axis

$F$ = strain compatability factor

$p$ = $A_s/bd$ = reinforcement ratio

$P_b$ = lateral binding ratio; ratio of volume of confinement reinforcement to the volume of bound concrete

$q_u$ = ratio of ultimate equivalent confined concrete stress to the limiting plastic compressive stress

$q_l$ = ratio of equivalent confined concrete stress to the limiting plastic compressive stress

$K_u$ = ultimate equivalent concrete stress factor; ratio of ultimate equivalent concrete stress to the unconfined cube compressive strength

A.2 Flexural Strength of Bound Concrete Beams

The following discussion is based on the assumption that the bound concrete stress-strain relationship, shown in FIGURE A.1 is known.

The conditions of stress and strain for a bound prestressed beam, reinforced in tension only, are shown in FIGURE A.2. With reference to FIGURES A.1 and A.2, it can be seen that the equivalent concrete stress may be expressed in terms of the plastic concrete stress.

$$f_{cu}'' = q_1 f_p$$

Because the compressed region of the beam is circular after spalling, the total compressive force cannot be calculated using the ordinary rectangular beam analysis. The area of confined compressed concrete, $A_{cc}$ can be expressed in terms of $K_u d$ and b , using the properties of a circle. Because the expression is complex and also changes for the particular type of spiral used, it shall not be derived and presented.

The analysis, based on a knowledge of the factors discussed above, could be carried out in the following manner:

(1) The ultimate moment may be determined by taking moments about the compressive force C, shown in FIGURE A2:

$$M_u = A_s f_{su} d(1 - K_2'' K_u'')$$

(2) From a summation of forces in the longitudinal direction, the expression,

$$f_{cu}'' A_{cc} = A_s f_{su} = pbd\ f_{su}$$

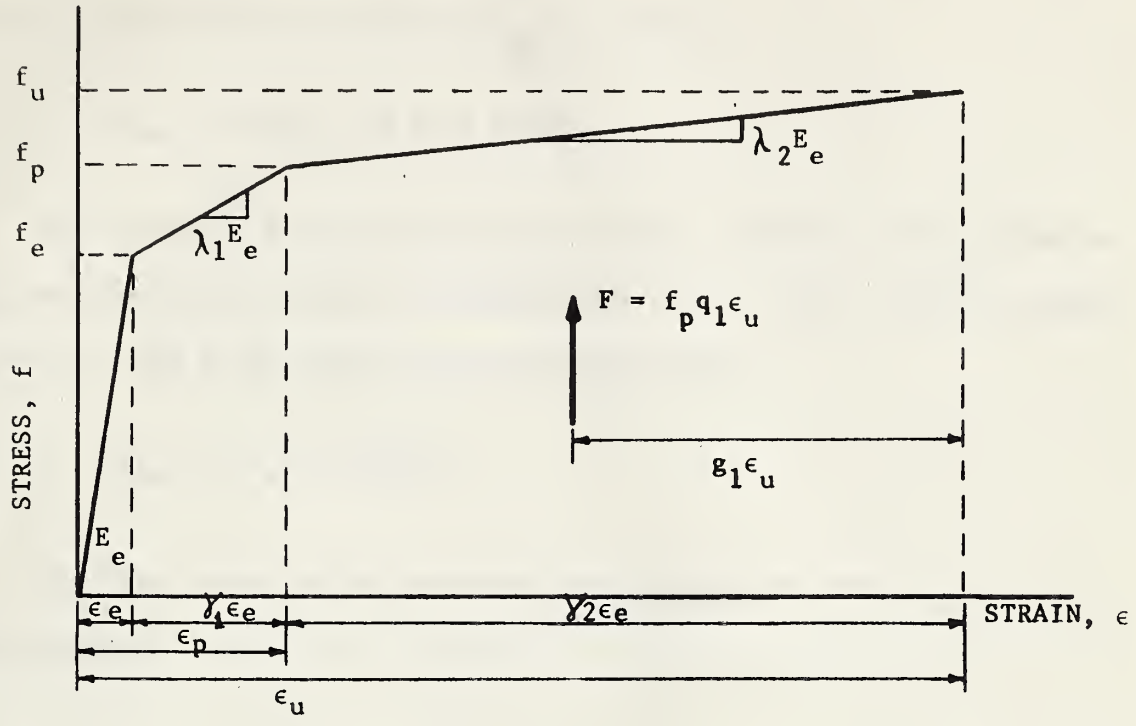


FIGURE A.1 GENERAL STRESS-STRAIN RELATIONSHIP FOR BOUND CONCRETE

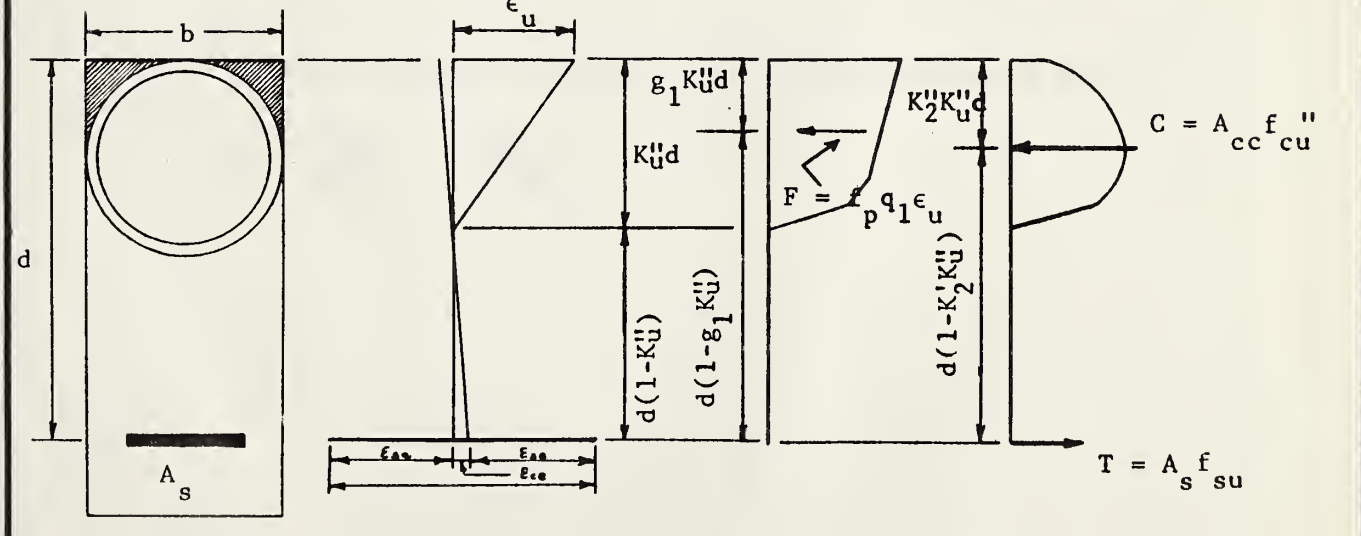


FIGURE A.2 CONDITIONS OF STRESSES AND STRAINS AT FAILURE

can be used to determine the value of $K''_u$ when:

$$A_{cc} = f(K''_u d) \quad \text{and } d \text{ is known.}$$

(3) From the strain distributions shown in FIGURE A.2 the relationship between the increase in reinforcement strain, $\epsilon'_{sa}$, and the concrete strain $\epsilon_u$ can be written in the following manner:

$$\epsilon'_{sa} = F\,\epsilon_u \left(\frac{1 - K''_u}{K''_u}\right)$$

(4) The strain in the tension reinforcement at failure, $\epsilon_{su}$, then becomes:

$$\epsilon_{su} = \epsilon_{se} + \epsilon_{ce} + \epsilon'_{sa}$$

(5) The two preceding equations can be combined to give:

$$\epsilon_{su} = \epsilon_{se} + \epsilon_{ce} + F\epsilon \left(\frac{1 - K''_u}{K''_u}\right)$$

(6) Average curvature at failure, $\phi_u$, may be obtained from:

$$\phi_u = \frac{F\epsilon_u}{K''_u\, d} \qquad \frac{\epsilon'_{sa}}{d - K''_u d}$$

# Appendix B

# METHODS OF CALCULATION

## B.1 Approximate Curvature Based on Deflections

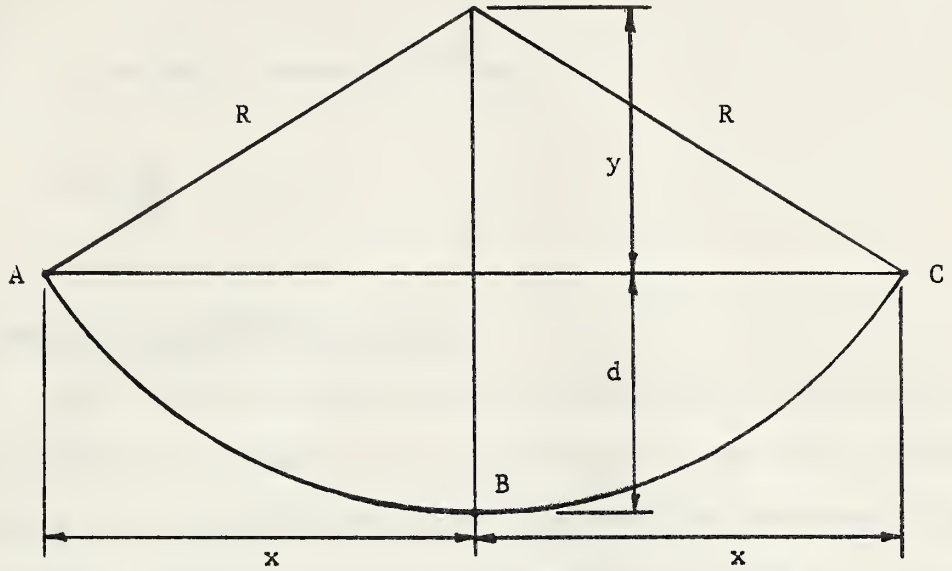


From above:

$$R^2 = x^2 + y^2 \qquad (1)$$

if d = relative deflection between line AC and point B then

$$R = y + d$$

or $$y = R - d$$

and $$y^2 = R^2 - 2Rd + d^2 \qquad (2)$$

Substituting (2) into (1) to get:

$$R^2 = x^2 + R^2 - 2Rd + d^2$$

$$R = \frac{x^2 + d^2}{2d}$$

therefore $\emptyset = \frac{1}{R} = \frac{2d}{x^2 + d^2}$ (3)

d is small, therefore $d^2 \longrightarrow 0$

and $\emptyset = \frac{2d}{x^2}$

B.2 Computation of Prestress Loss

The loss of prestress from the tensioning of cables until the time of test of the beam was due to relaxation of the steel, elastic shortening of the concrete at release and creep and shrinkage of concrete during curing. Measured losses are summarized in TABLE B.1, as well as initial prestress and effective prestress.

The initial prestress was measured with the dynamometers and strain indicator at the time of prestressing the strands. The strain indicator values were again obtained prior to release of strands. The loss, due to relaxation of the steel, was therefore the difference in these readings. A Demec gage line at the level of the steel was used to determine the elastic shortening of the beam during transfer of prestress. The Demec gage line was again read just prior to testing to evaluate the loss of prestress due to creep and shrinkage of the concrete during curing. The total loss of prestress was therefore known and could be used to determine the effective prestress in the strands at the time of testing.

TABLE B.1

SUMMARY OF PRESTRESS LOSSES

| Beam No. | Average Initial Prestress (ksi) | Average Steel Relaxation (in/in) | Average Steel Relaxation (ksi) | Average Elastic Shortening (in/in) | Average Elastic Shortening (ksi) | Average Time Loss (in/in) | Average Time Loss (ksi) | Effective Prestress (ksi) |
|---|---|---|---|---|---|---|---|---|
| A1 | 194.1 | 0.00051 | 14.3 | .00051 | 14.3 | .00066 | 18.5 | 147.0 |
| A2 | 182.6 | .00032 | 8.8 | .00034 | 9.6 | .00085 | 23.8 | 140.4 |
| A3 | 183.8 | .00037 | 10.3 | .00049 | 13.7 | .00103 | 28.9 | 130.9 |
| A4 | 190.7 | .00044 | 12.4 | .00073 | 20.6 | .00104 | 29.2 | 128.5 |
| B1 | 194.1 | .00051 | 14.3 | .00052 | 14.7 | .00098 | 27.4 | 137.7 |
| B2 | 182.6 | .00032 | 8.8 | .00034 | 9.4 | .00081 | 22.7 | 141.7 |
| B3 | 183.8 | .00037 | 10.3 | .00048 | 13.4 | .00098 | 27.5 | 132.6 |
| B4 | 190.7 | .00044 | 12.4 | .00071 | 19.8 | .00101 | 28.3 | 130.2 |
| C1 | 194.7 | .00041 | 11.5 | .00056 | 15.6 | .00103 | 28.9 | 138.7 |
| C2 | 194.7 | .00041 | 11.5 | .00051 | 14.2 | .00102 | 28.7 | 140.3 |
| C3 | 190.9 | .00030 | 8.3 | .00074 | 20.6 | .00123 | 34.4 | 127.6 |
| C4 | 190.9 | .00030 | 8.3 | .00071 | 19.8 | .00116 | 32.5 | 130.3 |

B.3 Cracking Moments

The theoretical moment at flexural cracking was calculated using an "elastic" analysis. The modulus of rupture was determined for each test beam from tests of 3 1/2 x 4 1/2 x 16-in. control specimens. Because the value of modulus of rupture, as determined from these control beam tests, was found to be high, the following expression was used to determine a value of modulus of rupture in terms of the compressive strength (8) (5):

$$f_r = \frac{3000}{4 + \frac{12,000}{f'_c}}$$

This expression was derived from tests of larger specimens and gives a more close approximation of the actual value.

The expression for the moment at which flexural cracking occurred, in terms of the modulus of rupture, effective prestress and beam properties is:

$$M_{cr} = \frac{I}{y_b} \left( f_r + \frac{P}{A} + \frac{Pe}{I/y_b} \right)$$

where $y_b$ = distance from the centroidal axis to the extreme tension fibre.

Theoretical and measured values of cracking moments are shown in TABLE B2.

TABLE B.2

OBSERVED AND THEORETICAL CRACKING MOMENTS

| Beam No. | Observed $M_{cr}$ (kip.ft) | Theoretical $M_{cr}$ (kip.ft) |
|---|---|---|
| A1 | 37.2 | 37.4 |
| A2 | 27.5 | 29.3 |
| A3 | 25.5 | 26.4 |
| A4 | 30.7 | 32.4 |
| B1 | 31.8 | 35.7 |
| B2 | 27.8 | 29.3 |
| B3 | 24.2 | 26.4 |
| B4 | 24.9 | 32.6 |
| C1 | 35.2 | 35.8 |
| C2 | 34.0 | 36.1 |
| C3 | 31.5 | 32.6 |
| C4 | 28.2 | 33.1 |